Nanostructured Materials for Application in Electrochemical Capacitors

A Thesis

Presented to the Faculty of the Graduate School

of Cornell University

In Partial Fulfillment of the Requirements for the Degree of

Master's of Science

By

Kenville Hendrickson

January 2014

Abstract

Electrochemical capacitors (EC's) are currently being investigated as primary energy storage devices due to their high power densities. Nanostructured materials with high surface area have gained significant attention in ECs where surface contributions play a significant role in the optimization of electrode performance. ECs are classified as electrochemical double layer capacitors (EDLC) and pseudocapacitors. Here we investigate the effect of surface area, morphology, and crystal size of various carbon substrates and metal oxide nanofibers on EC performance.

To determine the performance in EDLC devices, the effects of morphology and pore size of various carbon systems are analyzed, which include at two types of carbon black powder samples, XC-72 and super-P, and three different graphene nanoribbons (GNR) samples. It is observed that, despite their relatively low surface area, GNRs exhibit a higher capacitance due to ease of dispersion compared with carbon black powder samples.

Nickel oxide (NiO) nanofibers were synthesized through the electrospinning process to investigate the interplay between crystal morphology and pseudocapacitance performance. Electrospinning of aqueous polymer solution with high metal precursor loading, followed by thermal treatment produced highly crystalline metal oxide nanofibers. The nanofibers exhibited a tunable crystal size which increased with thermal treatment. The calcined NiO fibers thermally treated at 800C exhibited a high capacitance of 500 F/g.

Finally, composite electrodes are investigated by combining the GNR samples with the NiO fibers obtained from thermal treatment at 600°C and 800°C to study the synergy between the metal oxide and GNR matrix. The inclusion of GNR increased the capacitance from ~ 500

F/g to ~650 F/g. Our experiments also revealed that the aspect ratio of metal oxide nanofibers and their dispersion are crucial in enhancing the EC performance. NiO crystal nanowires with small aspect ratio performed better in unfunctionalized GNR samples, while those with larger aspect ratios performed better with functionalized GNR.

BIOGRAPHICAL SKETCH

Kenville Hendrickson was born in the U.S. Virgin Islands on the island of St. Thomas. He lived in St.Kitts and Nevis, West Indies until the age of 11 when his parents emigrated to Houston, Texas. There he developed a love for math and science that ultimately lead to his decision to study Chemical Engineering at The University of Texas, at Austin. After completing his B.S. in 2010, Kenville worked as a research assistant at the Separations Department at The University of Texas before he decided to attend Cornell University to pursue his PhD in 2011. Currently, Kenville is a graduate student at Cornell University studying the use of nanostructured materials for energy storage applications.

DEDICATION

I dedicate this work to my parents. My mother, Rupertha Hendrickson, for teaching me the true meaning of love and being thankful. My Father, Eustace Hendrickson, for unwavering support and unconditional love.

ACKNOWLEDGMENTS

I would like to thank my advisor, Dr. Yong Joo, for all his guidance and support during my Master's defense. Dr. Joo has an uncanny ability to take students and push them to new limits previously untapped. His ability to foster a thought within my heart and mind pushed me to create the best and most promising results. The creativity and thought provoking nature in which he generated new ideas is astonishing. All of which have been essential to my development as individual and researcher. I am deeply grateful for him as a mentor and role model. I would also like to thank my committee member Dr. Tobias Hanrath for his valuable suggestions. Dr. Hanrath often provided a source for new ideas that could easily be applied to overcome some of the difficult challenges presented in my research.

My sincerest gratitude also goes to my colleagues and friends for their help and support: Dr. Nathaniel Hansen, Dr. Yong Seok Kim, Ghazal Shoorideh, and Dr. Jun Yin.

TABLE OF CONTENTS

LIST OF FIGURES

Chapter 1

Introduction

Nanomaterials

Nanomaterials are of increasing interest due to their size-dependent properties in the sub-micron region. Often these materials are synthesized to optimize crystal size and surface area contributions [1]. High surface area-to-volume ratios of nanomaterials allow for the design of materials by utilizing reactive surface sites and electrostatic electrode/electrolyte interactions where surface contributions tend to dominate [2]. For reactive surface sites, the increased surface area contributes to increased performance since reactions are often limited to the surface of the material. Electrostatic electrode/electrolyte surface interactions operate through the separation of charge at the interface between the solid electrode surface and liquid electrolyte [3]. Controlling the size of the solid electrode material whose surface area is accessible to the liquid electrolytes provides for the closest contact distance for electrode/electrolyte interaction. By optimizing the surface area through controlled nanomaterials, the separation of charge at the solid electrode surface can be optimized in the electrochemical double layer. It has also been shown that the properties of nanomaterials can be tuned to control the size of the crystal domain within nanomaterials [4]. By increasing or decreasing the size of crystals within nanomaterials one can change the physical properties of such materials. This illustrates that through the use of nanostructures one can synthesize nanomaterials with tunable surface area and electrical conductivity properties. Here we aim to study the effect that crystal size and morphology of nanomaterials on the performance in energy storage devices.

Nanomaterials cover a vast range of nanoscale designs and morphologies. Two prominent types of nanomaterials are nanoparticle and nanowire systems. Nanoparticles are nanomaterials

characterized by a spherical-like geometry. They are often described as high surface area materials due to their high surface area to volume ratio. Unfortunately, their small size tends to lead to particle aggregation, due to high surface energy and the high surface area to volume benefit can easily be lost [5]. To overcome this effect, surface functionalized groups are incorporated to increase the affinity to the solvent or the matrix. Alternatively, one can generate nanomaterials that are one-dimensional [6]. Surface functionalization of nanoparticles to increase the nanoparticle to solvent interaction decreases the effect of aggregation, but, the presence of those surface groups may also prevent or limit surface reaction. [7]. Therefore, to utilize the benefits obtained from nanomaterials, it is proposed to synthesize one-dimensional materials, which are less prone to aggregation.

Electrochemical Deposition

A common method to synthesis one dimensional metal or metal oxide nanowires is electrodeposition [8]. This method often utilizes a nano-porous template, such as an anodized aluminum oxide or glass membrane, used to fill the pores which create anisotropic multilayer nanowire arrays. The use of a nano-porous template in the electrodeposition process leads to the creation of nanotubes and nanorods of similar size. The size and location of these pores creates nanowires of similar size that are collected after the template is removed. The nanowires must then be removed to collect free standing nanowires.

Nanowires produced from this method have many benefits. The nanowires synthesized have fixed control diameter, single crystalline material, and tunable crystal structure based on temperature and pressure. However, these processes also have two key disadvantages [9]. The process often occurs at small catalytic sites that, while successful in small scale processes, have

trouble with scalability to industrial applications. Furthermore, these processes tend to be fairly expensive. In addition, growing on a template dictates that the length or aspect ratios of the fibers are finite or low aspect ratio. This has lead to the need for a process that is easily scalable and relatively inexpensive.

Electrospinning process to synthesize One Dimensional nanomaterials

One way to overcome the disadvantages of the electrochemical deposition is to employ an electrospinning process to synthesize one-dimensional nanostructures [10]. The electrospinning process creates nanostructures or nanofibers by utilizing the complex viscoelastic properties of polymeric liquids. Electrospinning is an old process first invented in 1745 by Bose *et al* [11]. Despite its relatively long history, electrospinning was not readily utilized until the work of Reneker *et al.* in the early 1990s [12, 13]. Due to the elongation characteristics of the polymer, one can create fibers of varying diameter from the micron to submicron scale, by controlling the viscosity. Initially electrospinning was used for the synthesis of polymer nanowires such as polyethylene oxide and polyamide, but currently electrospun metal and metal oxide nanowires have experienced increased interest for nanomaterials synthesis.

In the electrospinning process, a polymer or polymer/precursor solution is fed through a thin metallic spinneret where it is extracted to a collector under the force of a high electric field (1 ~ 5 kV/cm) between the spinneret tip and the electrically conductive collector. The electric field induces repulsive forces that, once overcome by the surface tension of the fluid, produce a linear jet that flows towards the collector. The jet then goes thorough a bending and whipping motion where the fibers begin to elongate and stretch further as the solvent evaporates. Finally, the nanofibers are collected on a collector as a randomly oriented mat, and utilized for characterization and chemical or thermal treatment.

Nanofibers produced through the electrospinning methods provide a clear set of advantages. The bending and whipping motion elongates the fibers to form semi-infinite length scales with incredibly high aspect ratios [14]. Furthermore, the electrospinning process can be synthesized through water-based processes that are environmentally benign and inexpensive [15]. Finally, it has been demonstrated that aqueous polymer solutions with high loading of metal precursors can be electrospun to tune the electrical conductivity and magnetic properties of the fibers as a function of crystal size [16].

In this thesis the electrospinning process is used to generate metal oxide nanofibers of varying morphology for electrochemical capacitors (ECs). Currently ECs are designed with high surface area carbon nanotubes that have been shown to significantly increase the capacitance due to the higher surface area when compared to traditional carbon powders. We investigate the added benefits gained through the inclusion of nickel oxide nanofibers.

Electrochemical Capacitors

ECs play a significant role in energy storage devices because of their ability to provide incredibly high power density. Compared to batteries, ECs have much higher power density and long cycle times. This is a result of the slow Faradaic (redox) reactions and phase changes that occur in batteries that tend to cause structural damage over time. In contrast, ECs utilize the storage of surface charges. Since ECs function solely on the movement of surface charges they tend to occur much faster. However, ECs have been limited in their ability to become primary energy storage devices due to their low energy densities when compared to batteries (Figure 1.1).

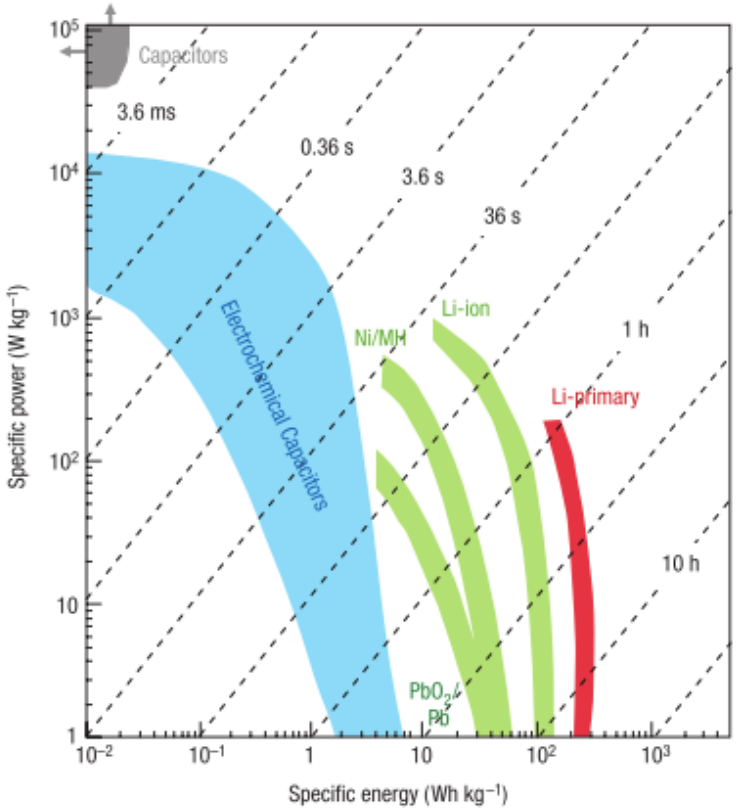

Figure 1.1 Ragone plot for various energy storage devices. Reproduced from reference [17]

Currently ECs are described as either electrochemical double layer capacitors (EDLC) or pseudocapacitors [18, 19]. EDLCs store energy as charge separation in the double layer formed at the interface between the solid electrode material and the electrolyte. This process is purely electrostatic and depends on the rapid adsorption and desorption of ions. In a typical EDLC, the cations of the electrolyte are attracted to the anode electrode due to electrochemical driving forces and the anions accumulate on the surface of the cathode due to the same charge process (Figure 1.2). The electrolyte ions approach the surface at a distance a little less than one nanometer to form the electrical double layer several nanometers thick. Charge separation occurs

through polarization at the electrode-electrolyte interface to produce the Helmholtz double layer capacitance C:

$$C = \frac{\varepsilon_r \varepsilon_0 A}{d} \tag{1.1}$$

Where ε_r is the dielectric constant of the electrolyte, ε_0 is the dielectric constant of the vacuum, d is the effective thickness of the double layer (charge separation distance) and A is the electrode surface area.

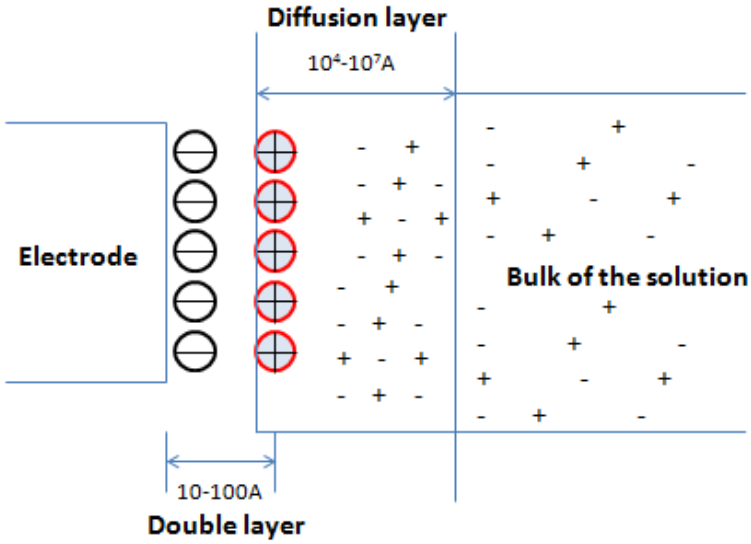

Figure 1.2 Schematic representation of electrochemical double layer interaction

Pseudocapacitors, in addition to the charge storage in EDLC, often involve slower electrochemical oxidation reduction reactions which can store 10-100 times more charge than EDLC [20]. Pseudocapaticors are faradaic in nature with most of the charge transferred at the surface or in the bulk near the surface of the solid electrode material. Applying a positive potential to the electrode lowers the energy level of the electrons. At a low enough level, the

electrons in the electrolyte solution find a thermodynamically favorable energy state on the electrodes and transfer to that location. The current used to transfer electrons from the solution to electrode is an oxidative current. Conversely applying a negative potential increases the electron energy level. At high enough energy levels, electrons transfer from the electrode into vacant electronic states on species in the electrolyte. Here the flow of electrons from electrode to solution is a reductive current [21]. Redox reactions often involve the use of metal oxides where metal ions have multiple valence state. As a result, materials such as nickel oxide, manganese oxide, and ruthenium oxide are favored to optimize both redox and ELDC mechanism [22-25].

When a potential difference is created between the two electrodes, equal and opposite charge develops on the two electrodes. The amount of charge on each plate, *Q*, is related to the applied voltage by:

$$Q = CV \tag{1.2}$$

The capacitance always varies as a function of charge. Therefore, the capacitance can be calculated from the current and slope from the discharge voltage curve:

$$C = \frac{Q}{V} = \frac{I}{(V/t)} = \frac{I}{-slope} \tag{1.3}$$

The capacitance can also be measured from cyclic voltammetry experiments. For an ideal capacitor, as the voltage is changed a constant current will be generated. The capacitance is then related to the current and the scan rate,v, where the scan rate is in units of volts per time.

$$C = \frac{Q}{V} = \frac{I}{(V/t)} = \frac{I}{v} \tag{1.4}$$

Important parameters in EDLC devices

Carbon is the most utilized material for electrode use in EDLC devices. They can be synthesized as powders, fibers, woven cloths and even porous sheets. The variety of methods available to synthesize carbon and the ability to produce materials with surface area as high as 2000 m^2/g makes it a promising candidate for current and future use. The abundant supply of carbon that currently exists, coupled with its low cost and good conductivity are important factors that are key to optimizing EDLC devices [26]. The varieties of ways in which carbon can be made include carbon black, active carbon, aerogels, and carbon nanotubes.

Activated carbon garners a significant amount of attention because they are relatively inexpensive, have high surface area, and have controllable porosity. They can be prepared with surface areas over 2000 m^2/g. Furthermore, the porosity can be controlled during the activation process. Since double layer capacitance is directly proportional to surface area, one would expect these materials to yield characteristically high capacitance values. However, for various reasons the correlation between surface area and capacitance does not always translate linearly. In fact, double layer capacitance has been shown to vary based on the different preparations of carbons from varying methods of processing to precursor treatments [27]. This can be seen in Table 1.1 shown below. Consequently, the variety of pores generated may not all be easily accessible to the electrolyte during the charging of the double layer. This is due to the surface area distribution of carbon, which consists of micropores (< 2 nm), mesopores (2 ~ 50 nm) and macropores (> 50 nm) [28, 29].

Table 1.1 Capacitance of various carbon nanomaterial. Reproduced from [27].

Material and method	Cell and evaluation method	Capacitance	Remarks [Ref.]
Activated carbon			
GC (air ox)	3E (3 m H_2SO_4) EIS	85–115 F mL^{-1}	Increase with oxidation time [24]
PFR (KOH ac)	2E (1 m H_2SO_4) CV	90–105 F g^{-1}	Increase with amount of KOH [25]
MP (KOH ac)	2E (1 m H_2SO_4) CV	130 F g^{-1}	Increase with amount of KOH [26]
PVDC (ht)	2E (30% H_2SO_4) CVC-GD	64 F g^{-1}	Max. at 700 °C, S_{BET} = 700 m^2 g^{-1}, no ac [36]
pitch, PFR, coconut (*nd*)	2E (1 m H_2SO_4, 1 m $LiClO_4$/PC) GCD	Fig. 1	Effect of pore size [17]
BM (steam or CO_2 ac)	2E (*nd* $TEABF_4$/PC) CVC-GD	17–33 F g^{-1}	Morphological effect [27]
c-AC (CO_2 ac)	2E (1 m $TEMABF_4$/PC) GCD	52 F g^{-1}	Increase by further ac [22]
Coal (KOH ac)	3E (1 m $LiClO_4$/PC) GCP	220 F g^{-1}	Max. at 700 °C [28]
Coal, PDC (KOH ac)	2E (1 m H_2SO_4) EIS, CV, GCD	200–320 F g^{-1}	Best performance with MP [29]
WC (CO_2 ac)	2E (1 m H_2SO_4) GCP	127–184 F g^{-1}	S_{BET} = 660–920 m^2 g^{-1} [30]
PVDF (KOH ac)	2E (1.2 m $TEABF_4$/PC) GCD, CV	39 F g^{-1}, 23 F mL^{-1}	Size effect of pore and solvated ion [31]
BM (ht)	2E (1 m H_2SO_4) CV, GCD	198 F g^{-1}	190 F g^{-1} after 6000 cycle [37]
BM, Polymers (ht, ac)	3E (7m H_2SO_4, KOH) CV	279 F g^{-1}, 267 F g^{-1}	Performance at room temp and −40 °C [33]
PDC (KOH ac)	2E (2 m H_2SO_4) GCD	400 F g^{-1}	Structural change of pores [34]
BM (steam ht)	3E (1 m H_2SO_4) GCP	280 F g^{-1}	Simultaneous ht and ac, surface area affected by ht rate, retention more than 90% at 1 A g^{-1} [38,39]
c-AC (steam ac)	2E (1.2 m $TEMABF_4$/AN) CV	60 F g^{-1}	Increase by further ac [23]

Small pores, micro- and mesopores, in the electrode play a significant role in optimizing the performance of ECs by improving the area available for charge storage in both EDLC and pseudocapacitors. In carbon based electrodes the specific capacitance normalized to specific surface area (SSA) does not significantly increase as the pore size increases (Figure 1.3 Zone III and IV) [17]. The added benefit of increased surface area is diminished as larger pores are created. Huang *et al.* were able to study the effects of the mesopores by modeling the pores as cylinders to generate an equation for the specific capacitance [30] :

$$C/A = \frac{\varepsilon_r \varepsilon_0}{b ln(\frac{b}{b-d})} \tag{1.5}$$

where *b* is the pore radius and d is the distance of approach of the ion to the carbon surface.

In the micropore region, a significant increase in capacitance is observed (Figure 1.3 zone 1). This is attributed to solvation of ions [31, 32]. The loss of the solvation shells allows for a

closer approach between the electrolyte and the electrode surface. This changes the specific capacitance to [30]:

$$C/A = \frac{\varepsilon_r \varepsilon_0}{b ln(\frac{b}{a})} \tag{1.6}$$

Where a is the effective size of the ion (desolvated).

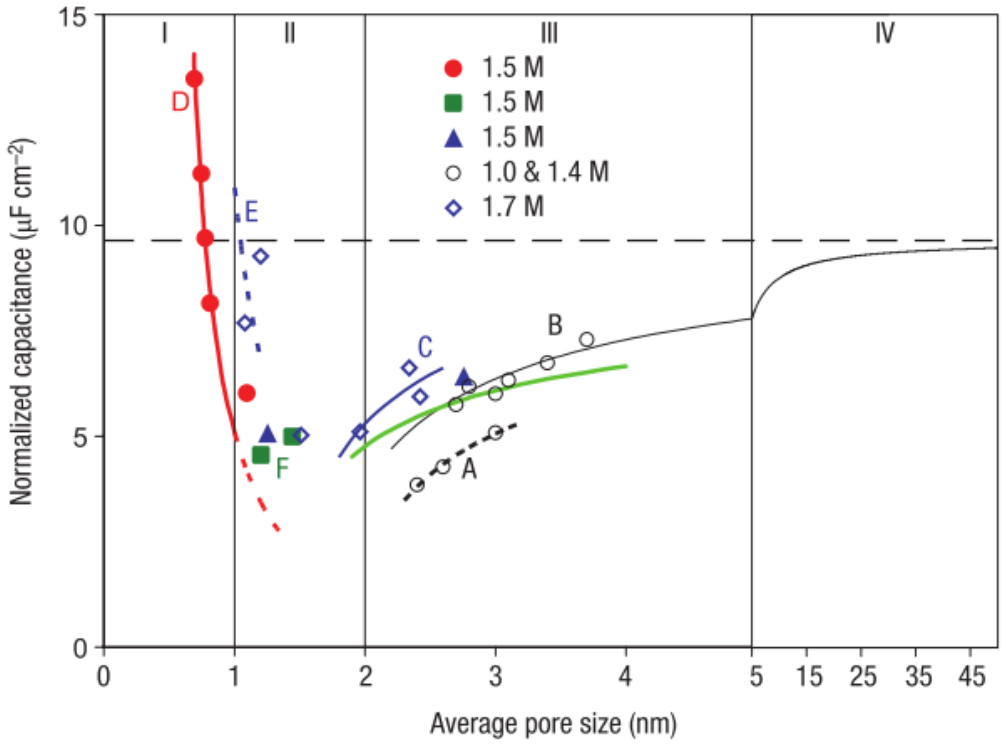

Figure 1.3 Specific capacitance normalized by SSA as a function of pore size. Reproduced from reference [17]

Carbon aerogels have high surface area, high pore volume, and good electrical conductivity [33-35]. They are synthesized from the pyrolosis of organic aerogels. Carbon aerogels have observed optimal capacitance performance when the pore size is between 3-13nm [27]. However aerogels are not favorable due to their high cost.

Carbon nanotubes (CNTs) are of high interest due to their mesoprous nature, good electrical conductivity, chemical stability, high mechanical strength, and high surface area between 100-400 m^2/g [36, 37]. Both single walled and multi-walled CNTs are viewed as excellent materials for EDLC devices [39, 40]. However, multi-walled carbon nanotubes (MWNTs) still suffer from low capacitance performance [37]. To improve the capacitance, chemical activation with KOH to increase the presence of micropores and the synthesis of MWNT composited with conducting polymers have been used. This has significantly increased the capacitance from ~70 F/g in MWNT to ~ 300 F/g for MWNT-oxides surface groups [38].

Important parameters in pseudocapacitive devices

In pseudocapacitors, the solid electrode/electrolyte interaction is based on reversible faradaic reactions. The charge transfer is voltage dependent. This means that the capacitance C :

$$C = \frac{dQ}{dV}$$

Pseudocapacitance is often a result of three kinds of electrochemical processes: surface adsorption of ions on electrode from electrolyte; reversible faradaic reactions involving ions from electrolyte; and doping and undoping of active conductive polymer electrode materials. Here we will focus on reversible faradaic reactions.

The incorporation of two or more intermediates is required to achieve a large constant capacitance. This is often achieved in systems that have multiple oxidation states and is known as redox (faradaic) pseudocapacitance. It has been shown that potential regions with multiple oxidation states have increased levels pseudocapacitance resulting in much higher capacitance values [site]. An ideal pseudocapacitor is conductive and has many oxidative states.

The most studied materials for redox pseudocapacitance are transitional metal oxides. Transition metal oxides are most suitable since they have multiple oxidation states and reasonable conductivity. Often studied metal oxides include RuO_2, MnO_2, and NiO.

Ruthenium oxide, RuO_2, is one of the most highly investigated metal oxides used for pseudocapacitance. In its crystalline form, it is a metallic conductor with good electrical conductivity and excellent catalytic activity as well as electrochemical and photochemical stability [41, 42]. Conway *et. al.* were the first to utilized crystalline RuO_2 as an electrode material for pseudocapacitors [43]. The highest reported value for RuO_2 was 380 F/g. The electrochemical analysis was fairly similar to an ideal capacitor with a reversible anodic and cathodic scan, and a near rectangular shape. Later work by Zheng *et al.* using amorphous RuO_2 demonstrated a high capacitance of 720 F/g in 1M H_2SO_4 electrolyte [44, 45]. They proposed that the bulk of the material is used for the H^+ ion intercalation in the amorphous system while the crystalline RuO_2 only utilized the surface or near the surface [46, 47]. Table 1.1 provides a brief summary of EC Materials and the optimized parameters associated with different EC device fabrication methods.

Table 1.2 Comparison of EC Materials

	EDLC		Pseudocapacitors		Hybrid capacitors	
Mechanism	EDLC		Redox reaction		EDLC, Redox, Intercalation	
Electrode	Activated carbon powder Activated carbon fiber Carbon aerogel		Metal oxides	Conductive polymers	Carbon, Metal oxides, Conductive polymers	
Electrolyte	Aqueous	Organic	Aqueous	Aqueous /Organic	Aqueous	Organic
Voltage (V)	1	3	1~2	1~3	2	4
Energy density (Wh/kg)	1~3	2~10	0.8~2	**3~10**	2~7	**8~15**
Power density (kW/kg)	0.8~5	0.5~3	0.5~4	**4**	0.8~**5**	0.5~**5**
Sp. surf. Area (m^2/g)	1,500 ~ 3,000		90 ~ 150	N/A	N/A	N/A
Sp. Capacitance (F/g)	100~200	40~80	300~**760**	400~**500**	100~200	40~80
Cost	Medium ~ high		**Very high**	low	Medium ~ high	

Goals of This Thesis Work

One dimensional nanowires can be utilized due to their high surface area contributions to optimize EDLC devices. Here we wish to investigate the effects of porosity and fiber morphology, crystal size contributions of nickel oxide fibers, and composite nickel oxide/ carbon systems for incorporation into EC devices. Controlling the pore size in carbon based ECs has been shown to drastically affect the capacitor performance. We begin by looking at the effect of pore size in carbon nanomaterials (CH.3). Then, we synthesize nickel oxide nanowires to investigate the effect of crystal size and fiber morphology on the capacitance (CH.4). Finally we conclude with composite carbon/nickel oxide systems to study the combined effect on overall performance (CH.5).

References

[1] Kan, S., Mokari, T., Rothenberg, E., & Banin, U. (2003). Synthesis and size-dependent properties of zinc-blende semiconductor quantum rods. *Nature materials*, *2*(3), 155–8.

[2] Park, M.-S., Kang, Y.-M., Wang, G.-X., Dou, S.-X., & Liu, H.-K. (2008). The Effect of Morphological Modification on the Electrochemical Properties of SnO2 Nanomaterials. *Advanced Functional Materials*, *18*(3), 455–461.

[3] Shukla, a. K., Banerjee, a., Ravikumar, M. K., & Jalajakshi, a. (2012). Electrochemical capacitors: Technical challenges and prognosis for future markets. *Electrochimica Acta*, *84*, 165–173.

[4] Tian, Z. R., Voigt, J. a, Liu, J., McKenzie, B., McDermott, M. J., Rodriguez, M. a, … Xu, H. (2003). Complex and oriented ZnO nanostructures. *Nature materials*, *2*(12), 821–6.

[5] Bonard, J., Stora, T., Salvetat, J., Maier, F., Stockli, T., Duschl, C., & Heer, W. A. De. (1997). Purification and size-selection of carbon nanotubes, (10), 827–831.

[6] Saleh, N. B., Pfefferle, L. D., & Elimelech, M. (2008). Aggregation kinetics of multiwalled carbon nanotubes in aquatic systems: measurements and environmental implications. *Environmental science & technology*, *42*(21), 7963–9.

[7] Bratlie, K. M., Lee, H., Komvopoulos, K., Yang, P., & Somorjai, G. a. (2007). Platinum nanoparticle shape effects on benzene hydrogenation selectivity. *Nano letters*, *7*(10), 3097

[8] Hulteen, J. C., & Martin, C. R. (1997). A general template-based method for the preparation of nanomaterials. *Journal of material Chemistry*, *1*, 1075–1087.

[9] Cao, G., & Liu, D. (2008). Template-based synthesis of nanorod, nanowire, and nanotube arrays. *Advances in colloid and interface science*, *136*(1-2), 45–64.

[10] Greiner, A., & Wendorff, J. H. (2007). Electrospinning: a fascinating method for the preparation of ultrathin fibers. *Angewandte Chemie (International ed. in English)*, *46*(30).

[11] G. M. Bose, Recherches sur la cause et sur la veritable theorie de l'ectricite, Wittenberg, 1745.

[12] J. Doshi, G. Srinivasan, D. Reneker, Polym. News 1995, 20, 206 – 207.

[13] D. H. Reneker, I. Chun, Nanotechnology 1996, 7, 216 – 223

[14] Huang, Z.-M., Zhang, Y.-Z., Kotaki, M., & Ramakrishna, S. (2003). A review on polymer nanofibers by electrospinning and their applications in nanocomposites. *Composites Science and Technology*, *63*(15), 2223–2253.

[15] Chronakis, I. S. (2005). Novel nanocomposites and nanoceramics based on polymer nanofibers using electrospinning process—A review. *Journal of Materials Processing Technology*, *167*(2-3), 283–293.

[16] Hansen, N. S., Cho, D., & Joo, Y. L. (2012). Metal nanofibers with highly tunable electrical and magnetic properties via highly loaded water-based electrospinning. *Small (Weinheim an der Bergstrasse, Germany)*, *8*(10), 1510–4.

[17] Simon, P., & Gogotsi, Y. (2008). Materials for electrochemical capacitors. *Nature materials*, *7*(11), 845–54. doi:10.1038/nmat2297

[18] Sun, G., Li, K., & Sun, C. (2010). Electrochemical performance of electrochemical capacitors using Cu(II)-containing ionic liquid as the electrolyte. *Microporous and Mesoporous Materials*, *128*(1-3), 56–61.

[19] Gao, H., Ting, Y.-J., Kherani, N. P., & Lian, K. (2013). Ultra-high-rate all-solid pseudocapacitive electrochemical capacitors. *Journal of Power Sources*, *222*, 301–304.

[20] Conway, B. E., Birss, V., & Wojtowicz, J. (1997). The role and utilization of pseudocapacitance for energy storage by supercapacitors. *Journal of Power Sources*, *66*(1-2), 1–14.

[21] B. E. Conway, Electrochemical Supercapacitor: Scientific Fundamentals and Technological Applications. New York: Plenum Publishers, 1999.

[22] Toupin, M., Brousse, T., & Be, D. (2004). Charge Storage Mechanism of MnO 2 Electrode Used in Aqueous Electrochemical Capacitor, (9), 3184–3190.

[23] Lee, S. W., Kim, J., Chen, S., Hammond, P. T., & Shao-Horn, Y. (2010). Carbon nanotube/manganese oxide ultrathin film electrodes for electrochemical capacitors. *ACS nano*, *4*(7), 3889–96.

[24] Deng, W., Ji, X., Chen, Q., & Banks, C. E. (2011). Electrochemical capacitors utilising transition metal oxides: an update of recent developments. *RSC Advances*, *1*(7), 1171.

[25] Nathan, T., Aziz, a., Noor, a. F., & Prabaharan, S. R. S. (2007). Nanostructured NiO for electrochemical capacitors: synthesis and electrochemical properties. *Journal of Solid State Electrochemistry*, *12*(7-8), 1003–1009.

[26] Kinoshita, K. Carbon: Electrochemical and Physicochemical Properties', John Wiley & Sons: New York, 1988.

[27] Michio Inagaki et al, *J.PowerSource*, 2010, 195, 7880

[28] Frackowiak, E.; Beguin, F. Carbon Materials for the Electrochemical Storage of Energy in Capacitors. Carbon 2001, 39, 937-950.

[29] Shi, H. Activated Carbons and Double Layer Capacitance. Electrochim. Acta 1996, 41, 1633-1639.

[30] Qu, D.; Shi, H. Studies of Activated Carbons Used in Double-Layer Capacitors. J. Power Sources 1998, 74, 99-107.

[31] J. S. Huang, et al., "Theoretical model for nanoporous carbon supercapacitors," Angewandte Chemie-International Edition, vol. 47, pp. 520-524, 2008.

[32 J. Chmiola, et al., "Desolvation of ions in subnanometer pores and its effect on capacitance and double-layer theory," Angewandte Chemie-International Edition, vol. 47, pp. 3392-3395, 2008.

[33] J. Chmiola, et al., "Anomalous increase in carbon capacitance at pore sizes less than 1 nanometer," Science, vol. 313, pp. 1760-1763, Sep 2006.

[34] 20. Mayer, S.T.; Pekala, R.W.; Kaschmitter, J.L. The aerocapacitor: an Electrochemical Double-Layer Energy-Storage Device. J. Electrochem. Soc. 1993,140, 446-451.

[35] Pekala, R.W.; Farmer, J.C.; Alviso, C.T. Carbon Aerogels for Electrochemical Applications. J. Non-Cryst. Solids 1998, 225, 74-80.

[36] Saliger, R.; Fischer, U.; Herta, C.; Fricke, J. High Surface Area Carbon Aerogels for Supercapacitors. J. Non-Cryst. Solids 1998, 225, 81-85.

[37] Li, C.; Wang, D.; Liang, T.; Wang, X.; Ji, L. A Study of Activated Carbon Nanotubes as Double-Layer Capacitors Electrode Materials. Materials Letters 2004, 58, 3774-3777.

[38] Ajayan, P. M. Nanotubes from Carbon, Chem. Rev. 1999, 99, 1787-1800.

[39] Ye, J. S.; Liu, X.; Cui, H. F.; Zhang, W. D.; Sheu F. S.; Lim, T. M. Electrochemical Oxidation of Multi-Walled Carbon Nanotubes and its Application to Electrochemical Double Layer Capacitors. Electrochem. Comm. 2005, 7, 249- 255.

[40] Pico, F.; Rojo, J. M.; Sanjuan, M. L.; Anson, A.; Benito, A. M.; Callejas, M.A.; Maser, W. K.; Martinez, M.T. Single-Walled Carbon Nanotubes as Electrodes in Supercapacitors. J. Electrochem. Soc. 2004,151, A831-A837.

[41] Honda, K.; Yoshimura, M.; Kawakita, K.; Fujishima, A.; Sakamoto, Y.; Yasui, K.;NishioN.; Masuda, H. Electrochemical Characterization of Carbon Nanotube/Nanohoneycomb Diamond Composite Electrodes for a Hybrid Anode of Li-Ion Battery and Super Capacitor. J. Electrochem. Soc. 2004,757 A532 -A541

[42]Trasatti, S.; Lodi, S. Electrodes of Conducting Metal Oxides. In Properties of Conductive Transition Metal Oxides With Rutile-Type Structures, Eds.; S. Trasatti, Elsevier, Amsterdam, 1980, pp. 301-358.

[43] Trasatti, S. Physical Electrochemistry of Ceramic Oxides. Electrochim. Acta 1991, 36, 225-241.

[44] Jordanov, S. H.; Kozlowska, H. A.; Vukovic, M.; Conway, B. E. Reversibility and Growth Behavior of Surface Oxide Films at Ruthenium Electrodes. J. Electrochem. Soc. 1978, 125, 1471-1480.

[45] Zheng, J. P.; Jow, T. R.; A New Charge Storage Mechanism for Electrochemical Capacitors. J. Electrochem. Soc. 1995,142

[46] Zheng, J. P.; Cygan, P. J.; Jow, T. R. Hydrous Ruthenium Oxide as Electrode Material for Electrochemical Capacitors. J. Electrochem. Soc. 1995,142, 2699-2703.

[47] Zheng, J. P.; Jow, T. R.; Jia, Q. X.; Wu, X. D. Proton Insertion into Ruthenium Oxide Film Prepared by Pulsed Laser Deposition. J. Electrochem. Soc. 1996, 143, 1068-1070.

[48] Zheng, J. P.; Jow, T. R. High Energy and High Power Density Electrochemical Capacitors Using Amorphous Metal Oxide Electrodes. J. Power Sources 1996, 62, 155-159.

Chapter 2

Experimental Methods

Nanofiber Electrospinning Setup

Solutions containing 9 wt. %, 78 kDa, 88% hydrolyzed PVA as purchased from Sigma were heated and stirred at 60 ℃ for 5 hours or until the solution was homogenous. The PVA solution was then mixed with metal acetate solution in 1:1 wt. ratio of PVA:Metal Acetate starting with 0.4 g PVA. The metal acetate solution was formed by mixing 0.4 g Metal acetate, 0.4 g de-ionized water, and 0.36 g Acetic acid. The metal acetate solution was also stirred for 5 h prior to combining the two samples. After the combined solutions mixed for 2 h, electrospinning was done using a Harvard Apparatus PHD 2000 Infusion syringe pump and a HV ES30P-5W Power Supply at 15 kV. The tip to collector distance was 15 cm, with a flow rate of 0.0065 ml/min through a 22 gauge stainless steel needle for monoaxial fiber formation. Once the fibers were collected, high temperature thermal treatment using a MTI Tube Furnace removed the polymer to form metal oxide nanofibers. A Scintag Theta-Theta X-ray Diffractometer (XRD) was used to detail crystal content, size and structure through X-ray diffraction patterns. Finally, a LEICA-440 Scanning Electron Microscope (SEM) was used to view nanofibers morphology and crystal structure. A schematic detailing the general electrospinning process is illustrated in Figure 2.1.

Material Synthesis

Metal:PVA loadings of 1:1 and 2:1 of nickel acetate and zinc actetate were electrospun and calcined at a ramp rate of $2/min$ to a maximum temperature of 500 then viewed under SEM to verify that fiber morphology was maintained after calcination. Furthermore, the fibers

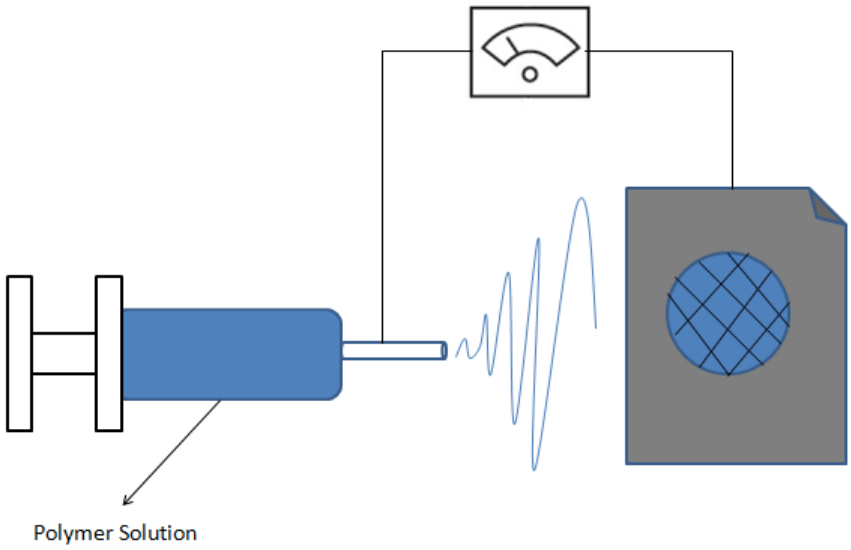

Figure 2.1. A schematic representation of Electrospinning setup.

were then analyzed under XRD to verify that after calcination Nickel oxide and Zinc oxide crystals were made and all the PVA was removed. The surface morphology, shown in Figure 2.2,

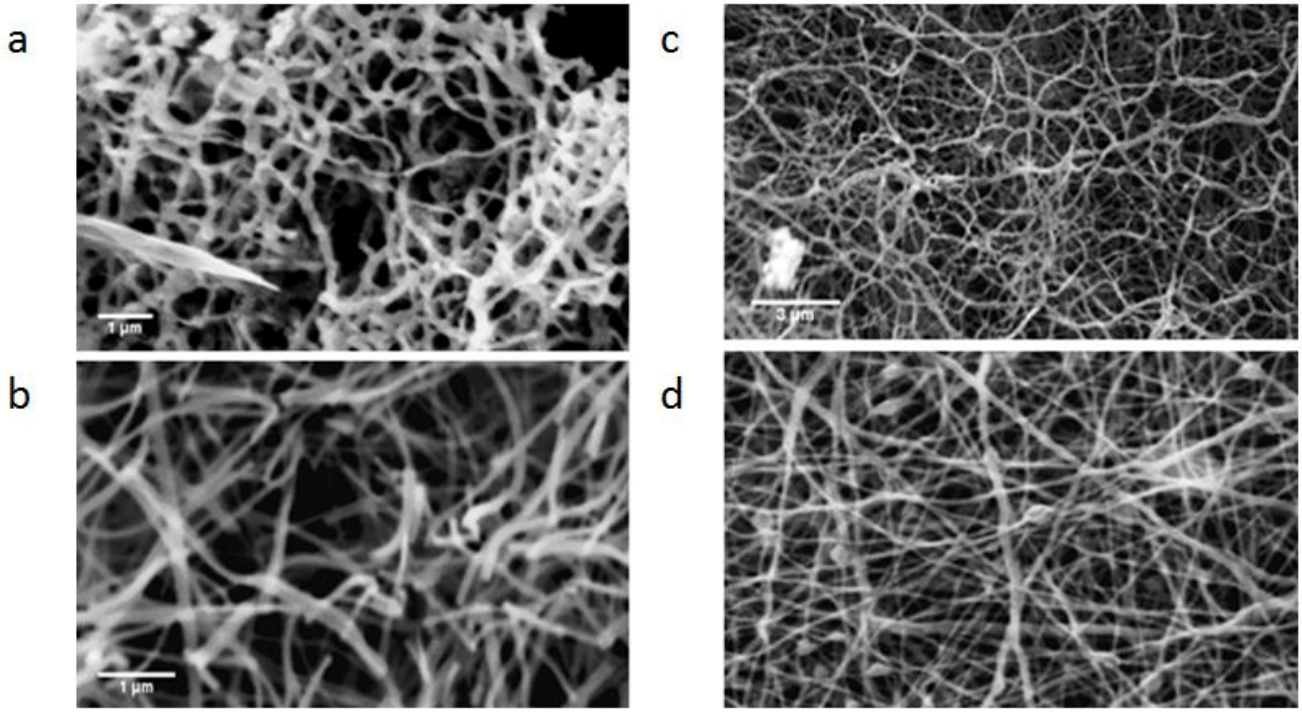

Figure 2.2 SEM image of 500 °C calcined samples of (a) 1:1 NiO, (b) 2:1 NiO, (c) 1:1 ZnO, (d) 2:1 ZnO.

illustrate that increased loading of metal:PVA precursor leads to better fiber morphology after calcination. Nickel oxide average diameter: (a) 142±32 nm and (b) 108±19 nm. Zinc oxide average diameter: (c) 123±30 nm and (d) 113±23 nm. Furthermore, XRD data shown in Figure 2.3 confirms formation of nickel oxide and zinc oxide crystals. XRD data for NiO peaks in

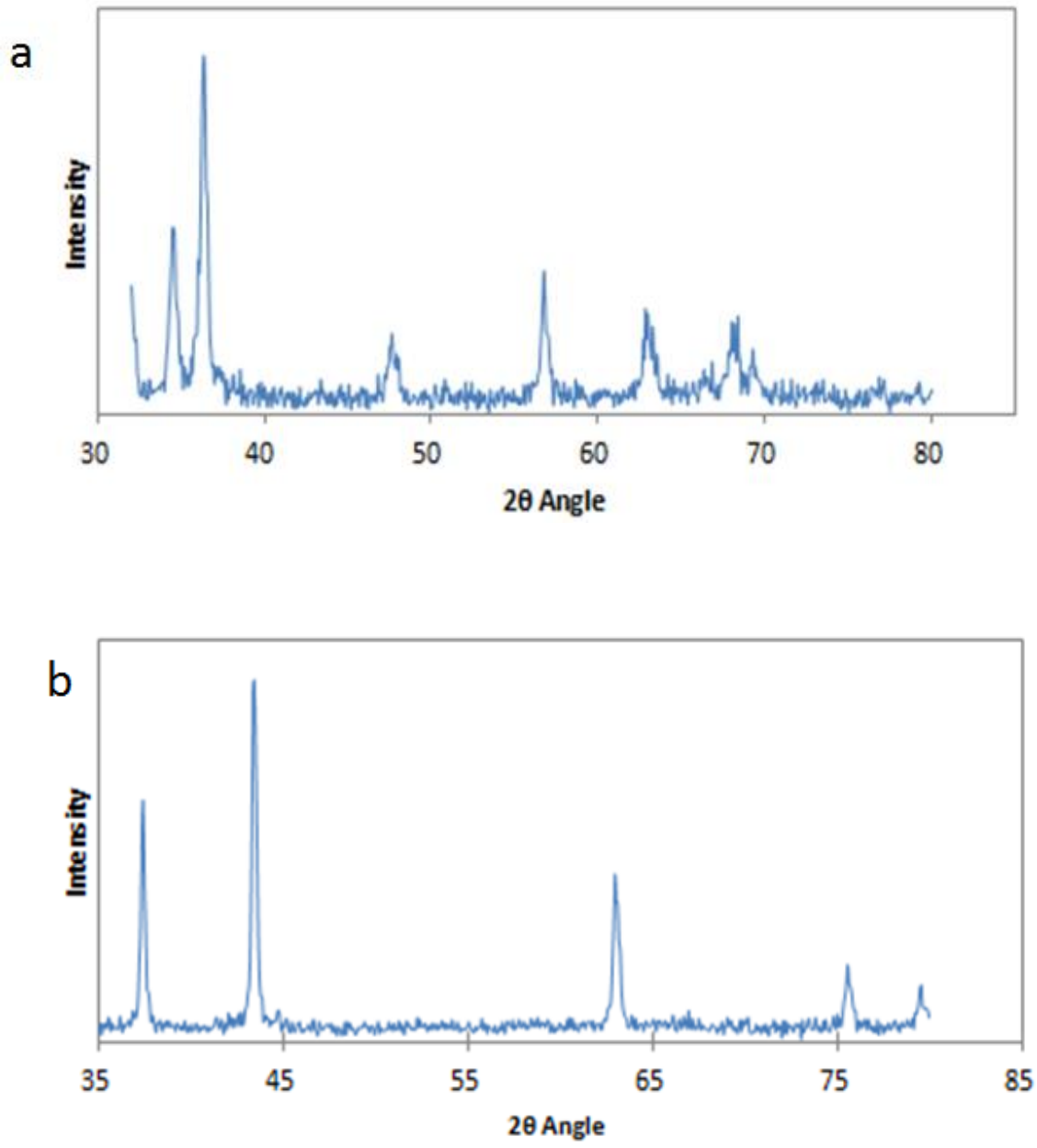

Figure 2.3 XRD data for (a) Zinc Oxide and (b) Nickel Oxide nanofibers calcined at 500 C.

Figure 2.3b are in good agreement with the known peaks which occur at 37.6, 43.7, 63.4, 75.7 and 79.8 degrees. Furthermore, copper oxide (CuO) and tin-doped-indium oxide (ITO) nanofibers were synthesized. The average diameter of ITO and CuO are 184±25 nm and 101±18nm respectively.The CuO fibers were syntheized using 1:1 metal acetate: PVA loading. The ITO nanofibers were synthesized using 1:2 metal acetate:PVA loading where the metal is composed of 0.05 tin acetate and 0.15 indium acetate. The SEM images and XRD data is presented in Figure 2.4 and 2.5 respectively.

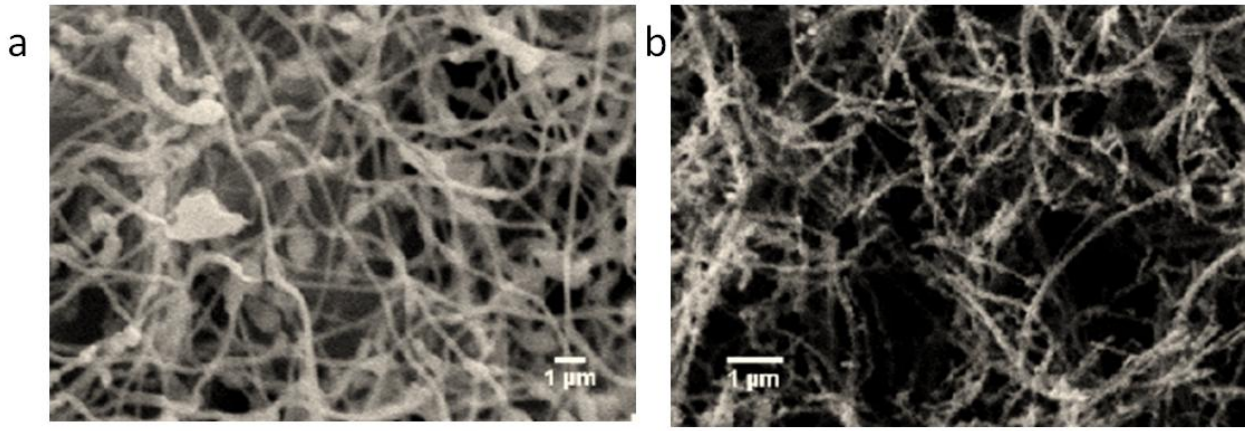

Figure 2.4 SEM image of calcined samples of (a) 1:2 ITO and (b) 1:1 CuO.

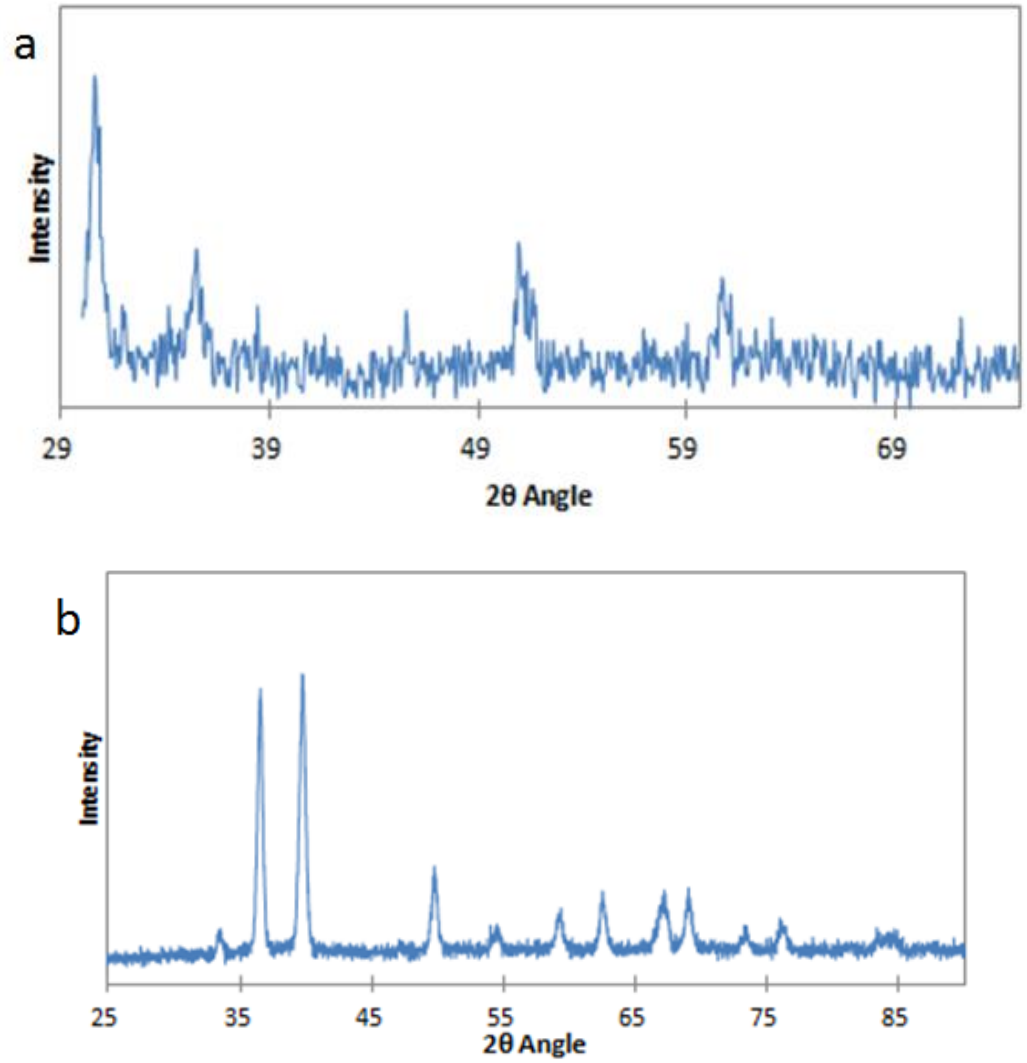

Figure 2.5 XRD data of image of calcined samples of (a) 1:2 ITO and (b) 1:1 CuO.

Three Electrode Setup

An open-beaker three-electrode cell, composed of the active material electrode as a working electrode, Ag/AgCl as the reference electrode, and platinum wire as the counter electrode comprised the experimental apparatus. Aqueous 3M KOH was used as electrolyte

solution. This experiment was designed to study the redox behavior of the synthesized nickel oxide fibers.

A schematic detailing the general setup of three-electrode cell is shown in Figure 2.6. Electrochemical measurements study the reactivity of the analyte as a function of applied potential. Here we limit our study to voltammetry experiments where the potential is varied continuously and the actual current is measured. In these experiments we control the potential of an electrode in contact with the analyte while measuring the current.

At least two electrodes are required to perform these experiments. A working electrode, which makes contact with the analyte, applies the desired potential in a controlled way to facilitate the transfer of charge to and from the analyte. A second electrode acts as the other half of the cell. This second electrode must have a known potential with which the potential of the working electrode is gauged. It must also balance the charge added or removed by the working electrode. Basically, this is a half cell test that measures the characteristics of the one of the electrodes in a controlled environment. However, two electrode setups are not often used since it is difficult for the reference electrode to maintain a constant potential while passing current to the counter redox events at the working electrode.

To solve this problem we introduce a third electrode to balance the charge added or removed by the working electrode, which is often an inert metal like platinum or silver. Now the reference electrode is a half cell with a known reduction potential whose sole purpose is to act as a reference in measuring and controlling the working electrode potential and it does not pass current. The third electrode, called an auxiliary or counter electrode, passes all the current to balance the current observed at the working electrode. To achieve this current, the auxiliary will

often swing to extreme potentials at the edges of the solvent window, where it oxidized or reduces the solvent or electrolyte [1-2].

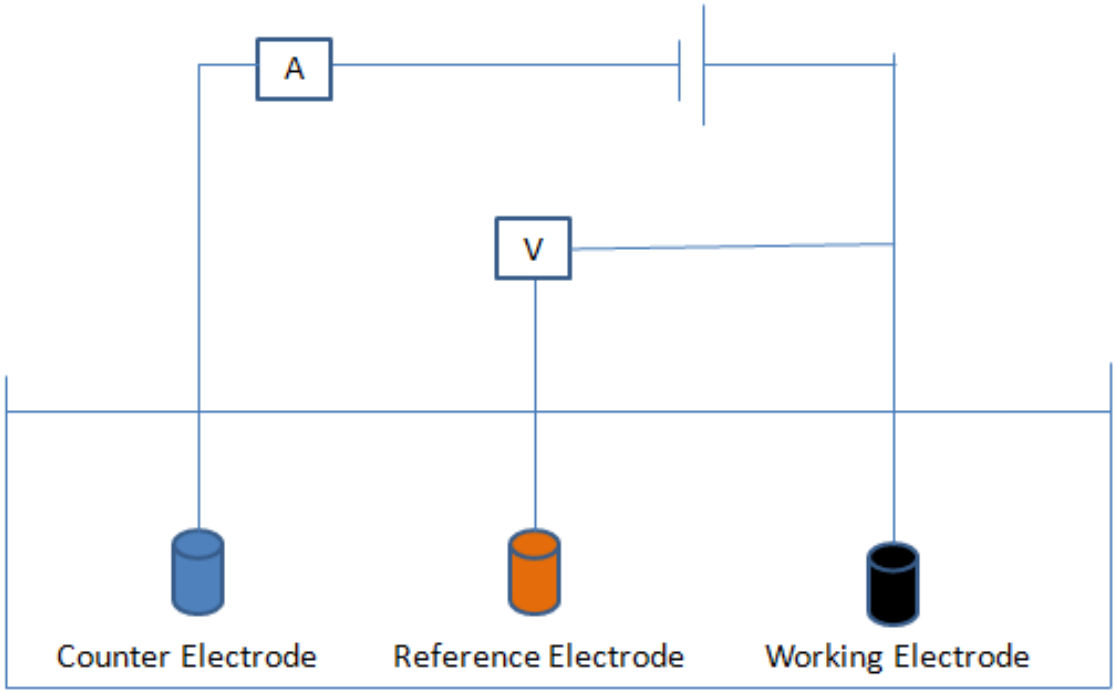

Figure 2.6 A schematic representation of Three Electrode System.

Reference

[1] E. Gileadi, Physical Electrochemistry, Fundamentals, Techniques and Applications. Weinheim: WILEY-VCH Verlag GmbH & Co. KGaA, 2011.

[2] A. J. Bard and L. R. Faulkner, Electrochemical Methods, Fundamentals and Applications. New York: John Wiley and Sons Inc., 1980. [11]

Chapter 3

Electrochemical Properties of Carbon Black and Graphene Nanoribbons for Electrochemical Double Layer Capacitors

Introduction

Electrochemical capacitors (ECs) are high power density materials used to facilitate the transition to next generation energy storage devices [1-2]. Currently ECs are investigated as possible energy storage systems to bridge the gap between batteries and conventional capacitors. Since they do not require chemical charge transfer reactions they are reversible which means they can in principle be cycled infinitely without loss of efficiency [1]. ECs that utilize carbon based materials are described as electrochemical double layer capacitors (EDLC). EDLCs store energy as charge separation in the double layer formed at the interface between the solid electrode material and the electrolyte. This process is purely electrostatic and depends on the rapid adsorption and desorption of ions.

In this chapter we attempt to analyze the physical parameters that contribute to increased EC performance. The charging of EDLC at the electrode/electrolyte interface can be significantly optimized through the incorporation of high surface area carbons. EDLC are not solely dependent on the surface area contributions but are also depends on the size and type or pores that exist [3, 4]. Therefore, a wide array of carbon-based materials like carbon blacks, carbon fibers, and nanotubes have gained considerable attention due to the ease at which nanomaterials of high surface area and high porosity can be fabricated [5-8]. Through the incorporation of highly developed surface area carbon black a specific capacitance as high as 300 F/g was achieved in the literature [6]. Furthermore, pore sizes in the range of micro-, meso-, and macro-pores all act differently as they diffuse the electrolyte to the inner surface of the porous

material [6, 9]. These physical aspects coupled with the morphology and structure has been shown to influence the chemical properties and capacitive properties of the carbon material.

To investigate these parameters, capacitive response of as received commercial carbon black Vulcan XC-72R (XC) powder is compared with novel graphene nanoribbon (GNR) structures. Three different graphene nanoribbon samples (GNR1, GNR2, GNR3) of varying pore distribution and surface area are compared to see the effect of pore contributions on capacitive performance. The GNRs were processed by different means to unzip the graphene nanotubes thereby creating graphene nanoribbons. GNR2 was just processed to unzip the graphene nanotubes. GNR1 is the same material as GNR2 functionalized with nanoclay prior to processing (shown in figure3.1). GNR3 went through further processing to unzip the nanotubes

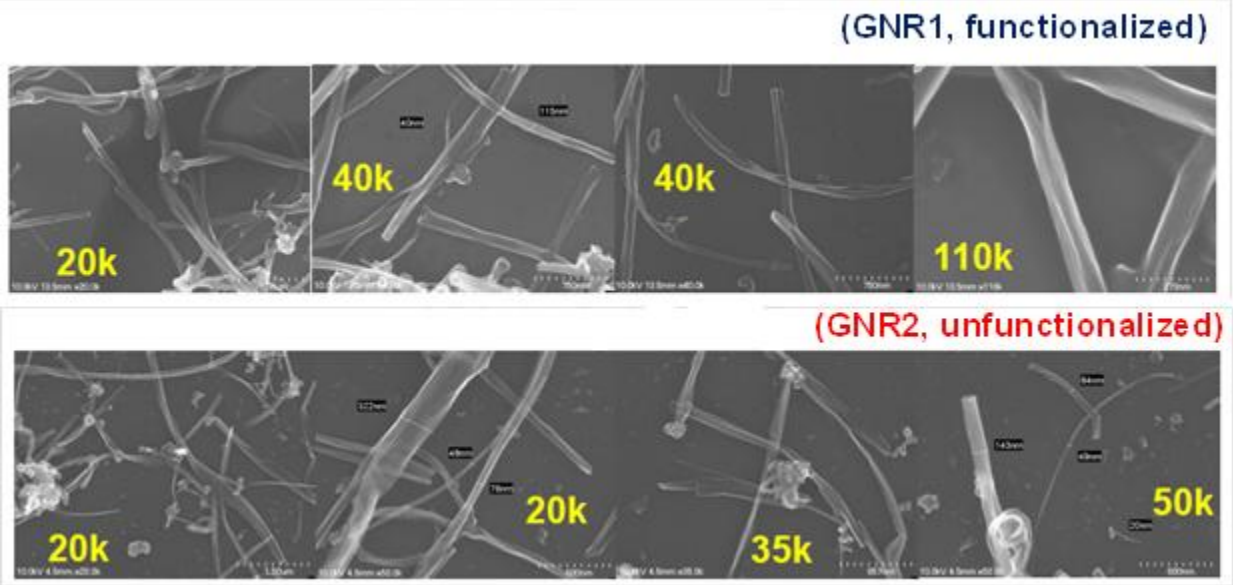

Figure 3.1 SEM images of GNR1 and GNR2 obtained from AZEM.

but without being functionalized. Here we investigate the effects of structural morphology changes due to powder and nanoribbons while looking at the effects of surface interactions attributed to the different morphologies after sonication. These four carbon materials are expected to show an enhancement of electrolyte accessibility to the internal surface of the layer.

Experimental Methods

The carbon black XC-72 powder was purchased from Cabot. The graphene nanoribbons were received from AZEM international. Sulfuric acid and isopropanol were obtained from Aldrich. All samples were used in their commercial form without further treatment or processing.

The specific surface area was calculated with the Brunauer-Emmett-Teller (BET) equation. Pore size distributions were calculated by the Barrett-Joyner-Halenda (BJH) method using the desorption branch of the isotherm. The surface morphologies of the XC-72 and GNR samples were further examined by scanning electron microscopy (SEM).

The working electrodes of the electrochemical capacitors were formed by mixing the active carbon material with 25% nafion onto a stainless steel substrate as the current collector. The active material was dispersed in isoproponal and layers were formed onto the substrate once the active material was homogenously dispersed after sonication. All electrochemical measurements were done in a three-electrode experimental setup. Platinum wire and Ag/AgCl were used as the counter and reference electrodes respectively. All measurements were carried out in 3 mol/L H2SO4 using a MTI-BST8 electrochemical workstation.

Results and Discussions

Prior to their use, the surface of the dry GNRs and XC-72 carbon black were analyzed using BET analysis and BJH to investigate the surface area and pore distribution respectively. The XC-72 sample has a highest surface area of 213 m^2/g. Each GNR was processed in a different manner to form the nanoribbons structure. This lead to the variation in surface area in Table 3.1. The processing of these

Table 3.1 Surface Characteristics of Carbon samples

Sample	Surface Area (m^2/g)	Diameter (nm)
XC-72	213	--
GNR1	38	133±20
GNR2	58	150±44
GNR3	72	157±23

GNRs also has a significant effect on the pore distribution of the samples. GNR1 is the only GNR that is functionalized, which attributed to it much smaller surface area and disparate pore size distribution compared to the other GNRs as seen in Figure 3.2. Furthermore, GNR2 and GNR3, which are unfunctionalized, have a significant localization of pores around 2-3 nm. This is in between the transition from micropores (<2nm) and meso-pores (>2nm) regions. However, XC-72 has a significant contribution of both small and large pores with a much larger localization of

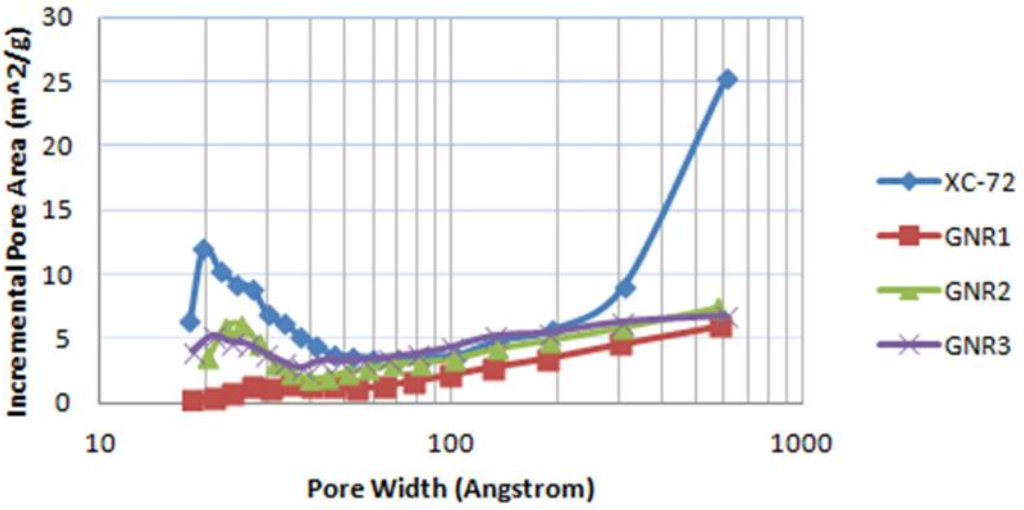

Figure 3.2. Pore size distribution of XC-72 and GNR samples.

pores close to the micron scale. One significant contrast between the two samples is the polydispersity of the samples. The XC-72 powder sample is composed of polydispersed particles but the GNR samples have monodispered diameters with varying surface area due to the processing of the GNR samples. The surface morphology of the samples can be seen in Figure 3.3.

The morphology of the various carbon systems are visualized under SEM. Figure 3.3 shows the morphology of the samples after sonication. There is a clear distinction between sample interactions of the XC-72 carbon black and the GNR systems. The XC-72 sample in its powdered form shows large aggregation of crystals with varying sizes, as illustrated in Figure 3.3a, while the GNR samples remain dispersed in their nanoribbon form without the presence of excessive aggregations. Due to the formation of nanoparticle agglomerate to form clusters the added benefit of high surface area XC-72 is diminished as many of those sites are no longer available to contribute to surface interactions. This indicates that the utilization of nanoribbons have an advantage of limited aggregation interactions. Furthermore, Figure 3.3b and 3.3c represent the unfunctionalized and functionalized version of the same GNR respectively. The functionalized GNR1 in Figure 3.3b demonstrated a diminished level of aggregation compared with unfunctionalized GNR2 in Figure 3.3c. Both the contribution of surface functional groups and the fiber morphology play a significant role in diminishing the occurrence of aggregation.

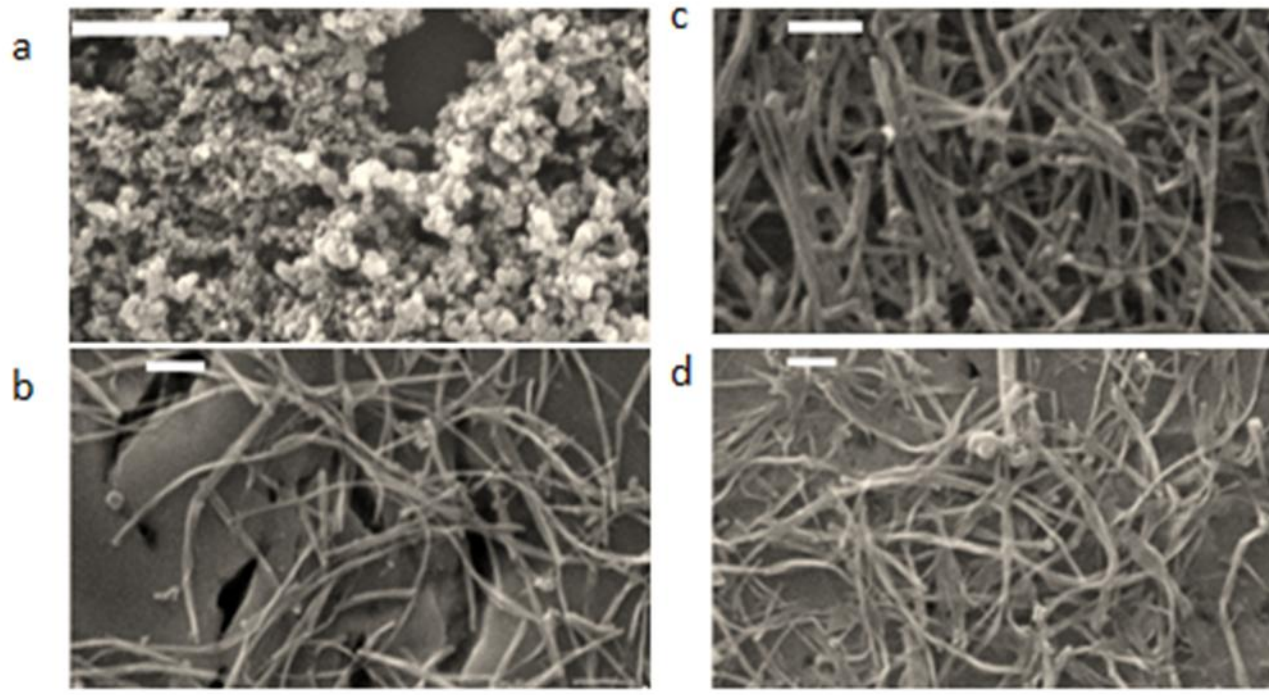

Figure 3.3 SEM images of (a) XC, (b) GNR1, (c) GNR2, and (d) GNR3. The scale bar in the top left corner is 1 µm.

To investigate the effects attributed to the processing of different GNR samples and compare the contributions of nanoribbons to the powder XC-72, the performance of the active materials were investigated using cyclic voltammetry (CV). Figure 3.4 shows the CV of GNR and XC-72 at various scan rates. It can be seen that the electrodes have near rectangular-shaped voltammograms, which is a characteristic feature of EDLC electrochemical capacitors. The increase of current with the scan rate indicates a good rate capacity for the electrodes at high

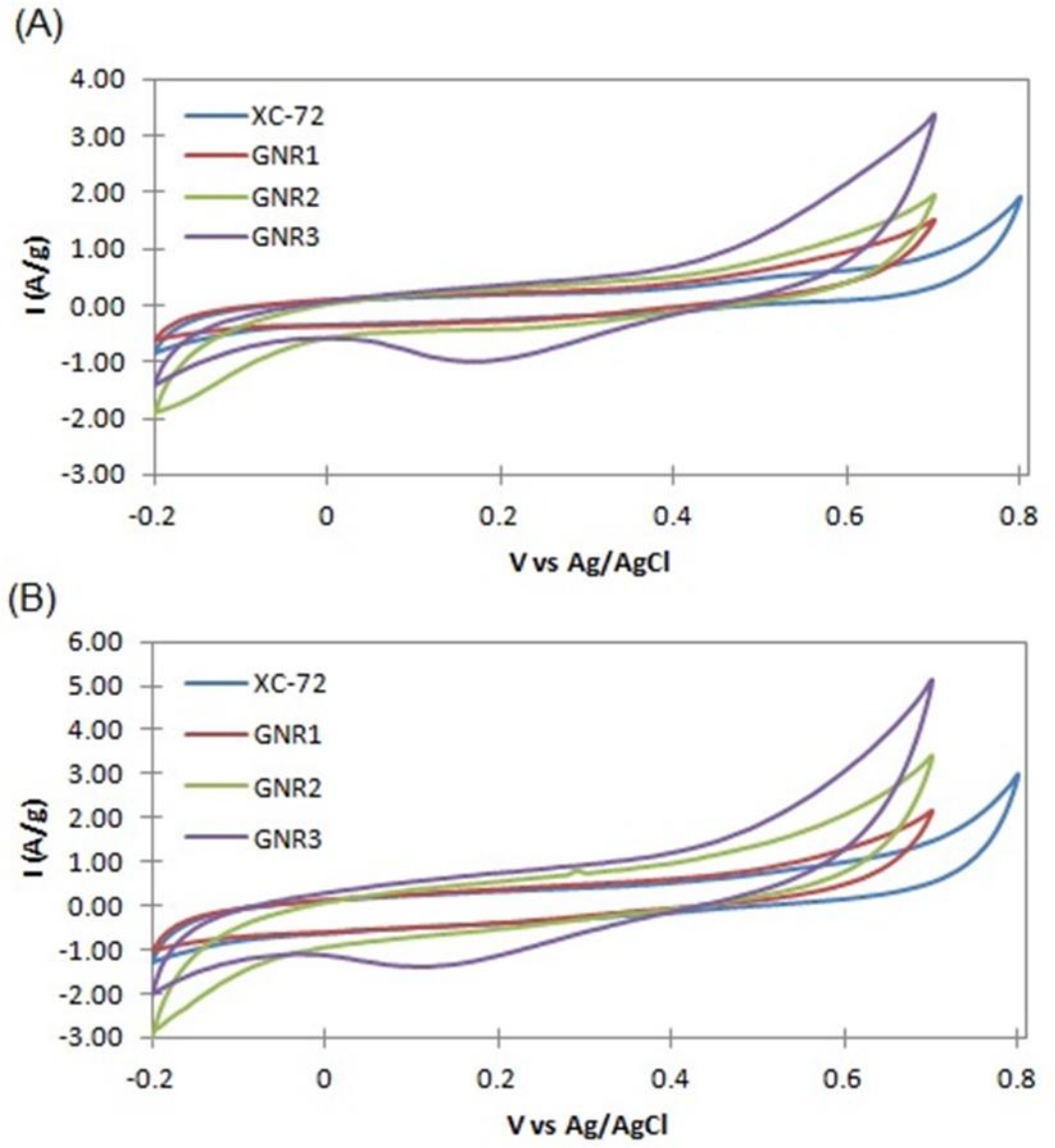

Figure 3.4. Cyclic voltammetry of the carbon samples at (a) 10mV/s and (b) 20mV/s.

scan rates. Furthermore, the GNR samples have better current performance compared with the XC-72 since the surface to electrolyte interactions were not limited due to aggregation. This is verified in Figure 3.3 where a larger separation of current and higher current values are observed for the GNR samples. This is due to increased interaction between the electrode surface and the electrolyte. XC-72 has similar characteristics has GNR1. This may be due to the fact that they

experience the same level of surface interaction with the electrolyte after sonication. The XC-72 sample aggregates, causing clusters to form which diminish the effect of the smaller pore sizes. This aggregation effect is seen in Figure 3.3a. As such, the surface area effect is decreased significantly. Although the GNR1 does not aggregate, the functionalized parameters limit pore size formation in the 2-3 nm range. The effect of functionalization created a similar effect of that to the aggregation of XC-72 powder. Current research has suggested that ELDC devices perform well when the inclusion of pore sizes between 2-3 nm is optimized and our results confirm this occurrence [10-14]. The GNR samples have much lower surface area compared to the powder XC-72. However, near negligible aggregation allows for better charge transport due to good interaction between the electrolyte/electrode surfaces.

The specific capacitance can be measured from the CV according to the following equation:

$$C = \frac{Q}{V \cdot m} = \frac{I}{(V \cdot m/t)} = \frac{I}{v \cdot m} \tag{3.1}$$

Where I is the current, v is the potential scan rate, m is the mass of the active material, and C is the double layer capacitance. For a given scan rate the current I is assumed to be constant leading to a constant value for C. Capacitance values are shown in Figure 3.5. The specific capacitance of the GNRs were higher than those of the XC-72 powder due to the improved porous features of the GNR between the 2-3 nm range and the lack of aggregation that hindered the electrolyte/electrode interaction of the EDLC. The XC-72 sample tends to aggregate after sonication leading to reduced surface area interaction. The functionalization of GNR1 decreased the localization of pores in the 2-3 nm range which hindered electrode/electrolyte interactions in a similar manner to XC-72. GNR2 and GNR3 are not hindered by these constraints and were

able to optimize the electrode/electrolyte interactions. This leads to high capacitance values for GNR2 and GNR3 around 60 F/g at 5 mV/s.

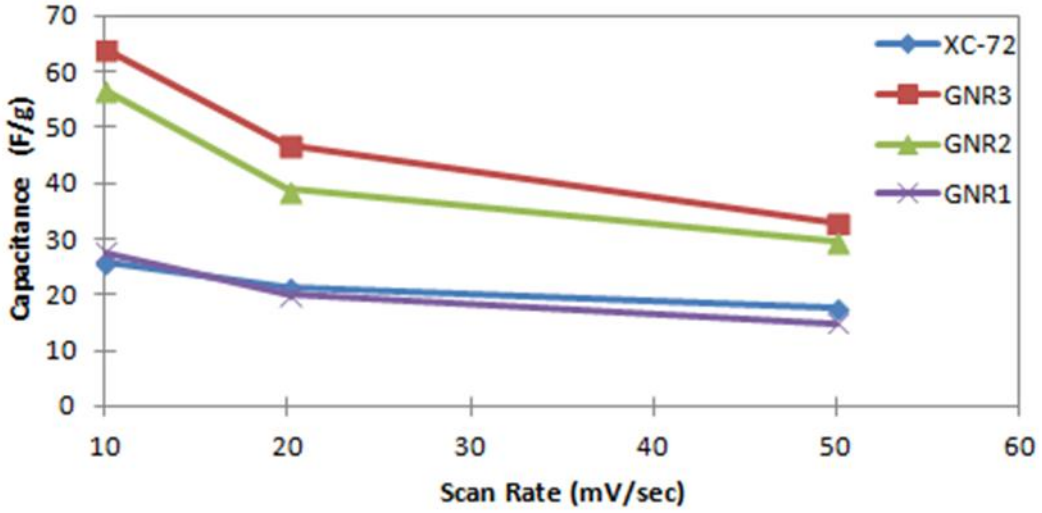

Figure 3.5 Average capacitance for (a) XC-72, (b) GNR1, (c) GNR2, and (d) GNR3.

The morphology of the carbon systems affects the surface characteristics of the electrodes used in EC devices. This is an interesting paradox because the variety of different processing techniques to synthesis carbon with high surface area is one of its biggest selling points. However, different processing methods affect the type of pore distributions created [15]. Here we have demonstrated that the morphology of GNR allows for fewer aggregation after sonication while the powder XC-72 aggregates to distort the actual amount of available pores. To further investigate this we extend our analysis to vary the morphology by comparing carbon black powder Super P-Li, GNR3, and MWCNT. The surface area for is 60, 71, and 177 m^2/g for Super P, GNR3, and MWCNT respectively. The Pore distribution is shown in Figure 3.6 and it can be seen that the carbon black has similar pore distribution to GNR as well as surface area.

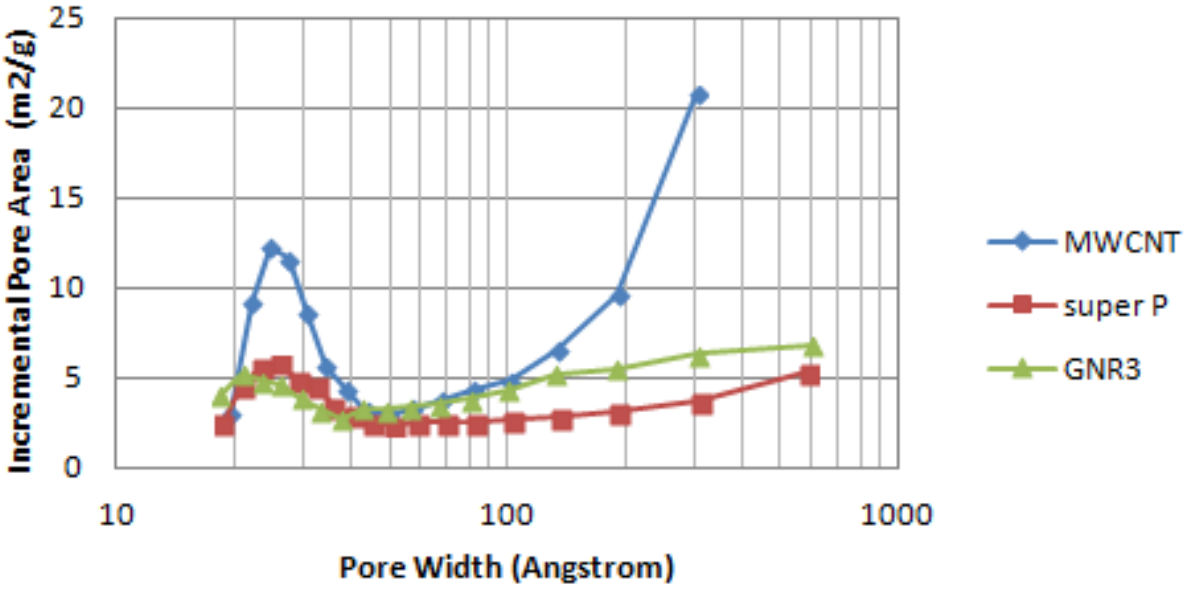

Figure 3.6 Pore size distribution of Super-P, GNR3, and MWCNT.

Furthermore, as we investigate the characteristic CV curves, the GNR and MWCNT samples perform drastically better compared to the super P carbon powder (Figure 3.7). This can be seen by the sharp separation in the anodic and cathodic current. The morphology of the MWCNT and GNR are fairly similar and as such their dependence on CV is fairly similar. GNR3 is simply a graphene nanotubes that were unzipped to form graphene nanoribbons. The much higher current output at a higher scan rate suggests good capacitance performance of the GNR3 and MWCNT and also suggest that the interaction between the surface of the electrode material and the electrolyte is being optimized. Characteristically low current for the Super-P powder suggest that surface electrode/electrolyte interactions are not being optimized possibly due to low surface area and aggregation effects seen in XC-72.

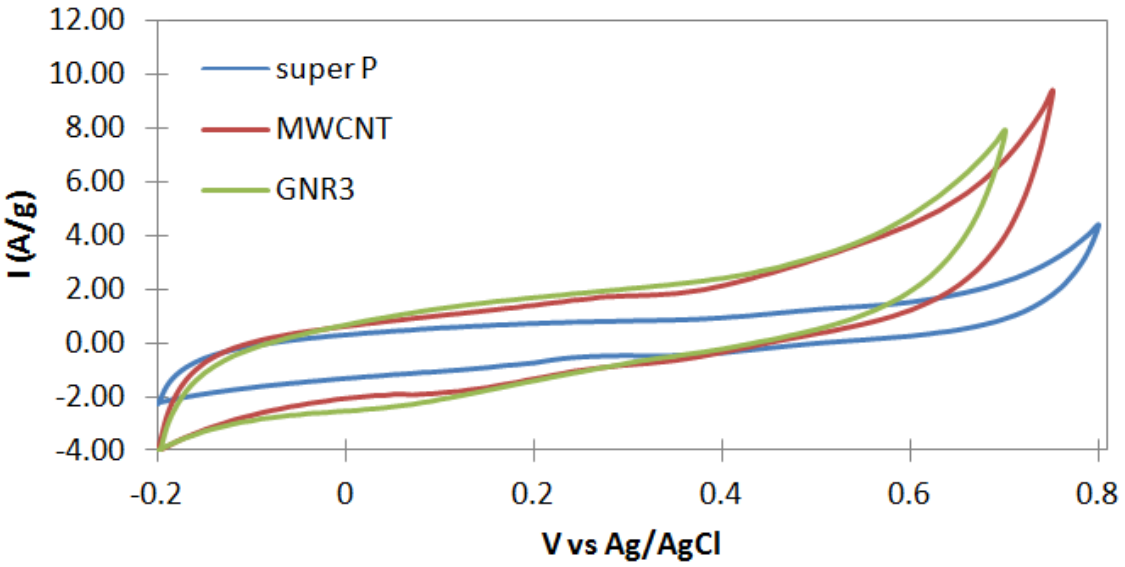

Figure 3.7 Cyclic voltammetry of the carbon samples at 50 mV/s.

A summary of the highest attained capacitance for the various carbon systems is presented in Table 3.2. As the morphology of the carbon electrode material changes so does the characteristic capacitance value obtained. Surface area contributions do not scale linearly with capacitance as processing changes that occur during sonication and other steps lead to significant changes in terms of surface morphology which significantly impact capacitance performance.

Table 3.2 Surface Characteristics of Carbon samples

Carbon Sample	Surface Area (m2/g)	High Capacitance (F/g)
XC-72	213	26
Super P	60	12
GNR1	38	28
GNR2	58	57
GNR3	72	64
MWCNT	177	37

Conclusion

Here we conclude two things: (1) surface area is not an independent event that leads to higher capacitance; (2) the degree of which the surface is affected due to processing plays a major role in limiting or allowing the added benefit of surface area to dominate. Capacitance behavior through the porous electrodes of carbon depends on their morphology and surface area. The morphology of the nanoribbons allows for limited aggregation leaving more sites available for electrode/electrolyte interaction within electrochemical double layer. Furthermore, the inclusion of pores between the 2-3 nm range seem to play a significant role in the effect of surface electrode/electrolyte interaction. The aggregated XC-72 sample tends to perform as well as GNR1 with limited 2-3 nm pores. This suggests that aggregation of particles tend to close up pore in the 2-3 nm range. Interesting enough this is around characteristic size of solvated ions which are generally interacting in the EDLC process.

Reference

[1] B. Conway, Electrochemical Supercapacitors—Scientific Fundamentals and Technological Applications, Plenum Publishers, NewYork, 1999.

[2] Ko, R., & Carlen, M. (2000). Principles and applications of electrochemical capacitors. *Electrochimica Acta*, *45*, 2483–2498.

[3] Largeot, C., Portet, C., Chmiola, J., Taberna, P., Gogotsi, Y., & Simon, P. (2008). Relation between the Ion Size and Pore Size for an Electric Double-Layer Capacitor, 2730–2731.

[4] Panić, V. V., Stevanović, R. M., Jovanović, V. M., & Dekanski, a. B. (2008). Electrochemical and capacitive properties of thin-layer carbon black electrodes. *Journal of Power Sources*, *181*(1), 186–192.

[5] J.-B. Donnet, R.C. Bansal, M.-J.Wang, Carbon Black Science and Technology, CRC Press, Boca Raton, USA, 1993.

[6] W. Zhu, D.E. Miser,W.G. Chan, M.R. Hajaligol, Carbon 42 (2004) 1841–1845

[7] B.M. Babi´c, B.V. Kaludjerovi ´c, Lj.M. Vra˘car, V. Radmilovi´c, N.V. Krstaji ´c, J. Serb. Chem. Soc. 72 (2007) 773–785.

[8] A.G. Pandolfo, M. Amini-Amoli, J.S. Killingley, Carbon 32 (1994) 1015–1019.

[9] A.G. Pandolfo, A.F. Hollenkamp, J. Power Sources 157 (2006) 11–27

[10] Shi, H. Activated Carbons and Double Layer Capacitance. Electrochim. Acta 1996, 41, 1633-1639.

[11] Qu, D.; Shi, H. Studies of Activated Carbons Used in Double-Layer Capacitors. J. Power Sources 1998, 74, 99-107.

[12] J. S. Huang, et al., "Theoretical model for nanoporous carbon supercapacitors," Angewandte Chemie-International Edition, vol. 47, pp. 520-524, 2008.

[13] J. Chmiola, et al., "Desolvation of ions in subnanometer pores and its effect on capacitance and double-layer theory," Angewandte Chemie-International Edition, vol. 47, pp. 3392-3395, 2008.

[14] J. Chmiola, et al., "Anomalous increase in carbon capacitance at pore sizes less than 1 nanometer," Science, vol. 313, pp. 1760-1763, Sep 2006.

[15] Frackowiak, E.; Beguin, F. Carbon Materials for the Electrochemical Storage of Energy in Capacitors. Carbon 2001, 39, 937-950.

Chapter 4

Nickel Oxide Nanofibers with Controlled Crystal Size for Enhanced Electrochemical Capacitor Performance

Introduction

Electrochemical capacitors have received considerable attention as power energy sources due to their high power density characteristics [1-4]. For ECs to be considered as primary energy storage device, high energy density must be achieved to balance the high power density that already exists in these devices. Typically, these devices incorporate high surface area carbon or metal oxide based materials [5,6].

Currently, a significant amount of research has focused to incorporate nanostructured electrodes as a means to enhance surface area leading to higher capacitance performance [7-9]. Although this is a viable approach, high surface area nanomaterials is not a simple solution that resolves all the issues associated with ECs. This is because ECs are not merely surface phenomena but also involves bulk contributions [10-12]. Here we wish to vary crystal size within highly loaded nickel oxide nanofibers to see the effects on the bulk for pseudocapacitance nickel oxide.

Pseudocapacitors often involve electrochemical oxidation reduction reactions which can store 10-100 times more charge than EDLC [13]. Pseudocapacitors are Faradaic in nature with most of the charge transferred at the surface or in the bulk near the surface of the solid electrode material. The interaction between the solid material and the electrolyte involve faradaic reactions. Transitional metals, such as nickel oxide, cobalt oxide, and manganese oxide, are often incorporated in pseudocapacitance devices due to their high level of oxidation states [14-18]. Most work studying bulk contributions with metal oxides has been done on the incorporation of nanoparticles and focusing on grain sizes or amorphous films [19-25]. The use

of amorphous ruthenium oxide was shown to significantly increase the capacitance by increasing the bulk contribution of materials that involved in the charge transfer. Furthermore, the incorporation of small nanoparticles was shown to be more efficient in creating a more continuous matrix for electron transfer compared to the large crystal particles with huge grain boundaries that limit efficient transport [26, 27]. In this paper nickel oxide nanofibers that are semi-infinite axially, were synthesized with large and small crystal domains structures to study their effect on pseudocapacitance. Recent work has shown that large continuous matrix within Ni metal fibers increased the conductivity due the continuous axial matrix available for electron transfer [28]. Using the same method to synthesize the fibers, followed by thermal treatment to create NiO fibers, this chapter aims to investigate the control of crystal morphology in NiO nanofibers.

Experimental Methods

Solutions containing 9 wt. %, 78 kDa, 88 % hydrolyzed PVA as purchased from Sigma were heated and stirred at 60 ^{o}C for 5 hours or until the solution was homogenous. This solution was then mixed with 1.6 g of nickel acetate to for a 4:1 Nickel to metal ratio. After these solutions mixed for 4 hours, electrospinning was done using a Harvard Apparatus PHD 2000 Infusion syringe pump and a HV ES30P-5W Power Supply at 15 kV. The tip to collector distance was 15 cm, with a flow rate of 0.0065 ml/min through a 22 gauge metal needle for monoaxial fiber formation. Once the fibers were collected, high temperature thermal treatment using a MTI Tube Furnace, heating and cooling rate of 5/min in air at a maximum temperature of 600 ^{o}C for 1 hour, was used to remove the PVA resulting in crystalline nickel oxide fibers. The maximum temperature was also changed to 400^{o}C and 800^{o}C to change the crystal size. A

Scintag Theta-Theta X-ray Diffractometer was used to detail crystal content, size and structure through X-ray diffraction patterns. Finally, a Tescan-Mira-3 FE Scanning Electron Microscope was used to view nanofibers morphology and crystal structure.

The nickel oxide electrode was prepared using a standard procedure by mixing NiO/Nafion/carbon black in 80:10:10 rations. The electrode was made by dispersing the above mixture in isopropanol and sonicated for 30 minutes to form a slurry. The slurry was then coated on a stainless steel current collector.

An open-beaker three-electrode cell, composed of the active material electrode as a working electrode, Ag/AgCl as the reference electrode, and platinum wire as the counter electrode was set-up. Aqueous 3M KOH was used as electrolyte solution. This experiment was designed to study the redox behavior of the synthesized nickel oxide fibers.

Results and Discussion

The XRD patterns of calcined NiO nanofibers show the formation of crystalline NiO, even at temperatures as low as 400^{o}C . However at 400^{o}C there is still residual presence of PVA precursor, which is completely removed after heat treatment at 600 ^{o}C as shown in Figure 4.1. The width of the Bragg reflection is considerably broadened for Figure 4.1a, indicating the formation of small domain size of crystals. The broadenings diminish with the increase of heat treatment temperatures, suggesting the growth of the NiO crystals. Figure 4.1b and c show sharp peaks due to the effect of heat treatment at 600^{o}C and 800^{o}C (1hour in air). As the heat treatment increases, the crystal structure of NiO is well established as seen by the sharp diffraction peaks demonstrating increased crystallinity within the sample.

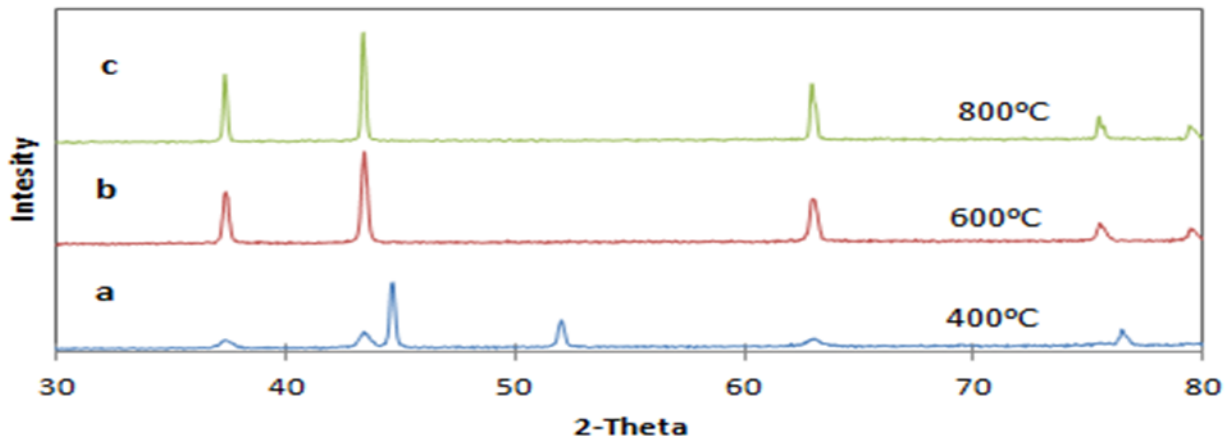

Figure 4.1 X-ray diffractograms of NiO at different heat treatment temperature.

The crystal size domain was calculated using Scherrer's equation. The estimated grain size using Scherrer's formula was found be around 20nm, 50nm and 150nm at 400, 600 and 800°C respectively. The grain size using XRD are smaller than those observed in the high resolution SEM. This is consistent, since Schrerer's equation does not take in to account broadening due to mechanical strain.

The nanostructure morphology of the calcined fibers was confirmed by FE SEM analysis. The average fiber diameter at 400°C, 600°C, and 800 °C were 300±30 , 270±60, and 250±20 nm respectively. Figure 4.2 clearly demonstrated that as the heat treatment temperature increases the particles grown significantly.

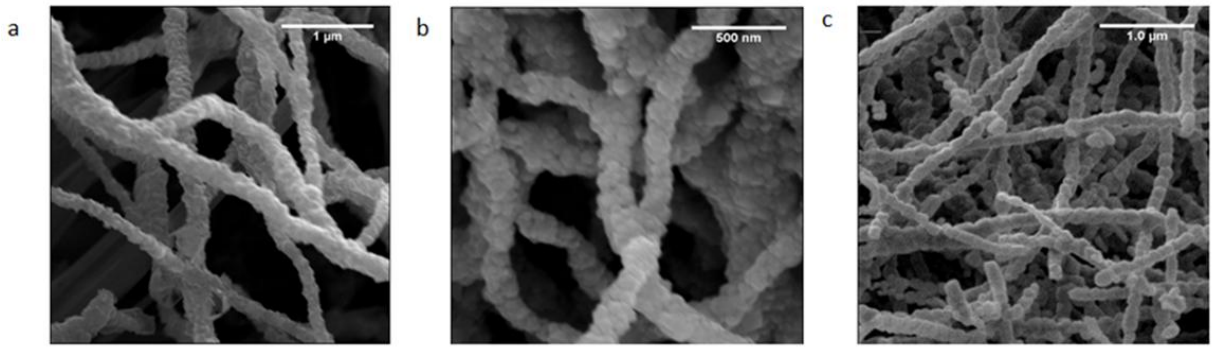

Figure 4.2. FE-SEM Pictures of NiO heated at a 400 °C , b 600 °C, and c 800 °C at 5°C /min for 1 hour in air

Cyclic voltammetry was used to determine the electrochemical properties of the synthesized NiO nanofibers in 3 M KOH solution. Nickel oxide calcined at 600 and 800 ºC were chosen for this study since all the PVA was removed at 600ºC. Figure 4.3 shows the rate dependent cyclic voltammetry (CV) of NiO vs Ag/AgCl. The electrode potential was scanned between 0.0 and 0.5 V vs Ag/AgCl in both anodic and cathodic directions while the current was measured. The redox features corresponding to anodic and cathodic peaks occur at ~0.38 and 0.26 V respectively at 5 mV/s in the 800 ºC NiO case. It is much more difficult to distinguish the clear flattening of the peak in the 600ºC case. The appearance of anodic and cathodic peaks

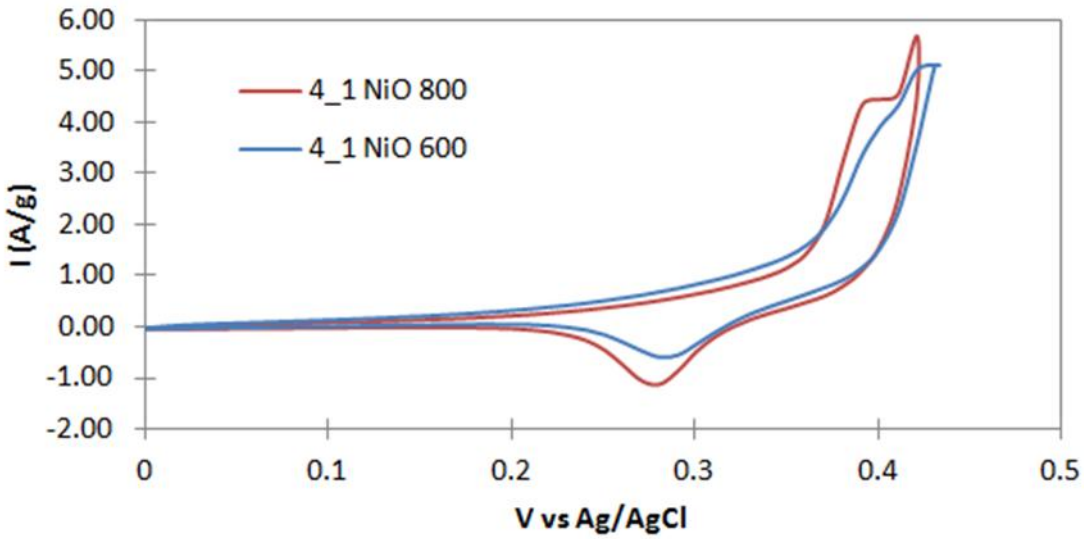

a

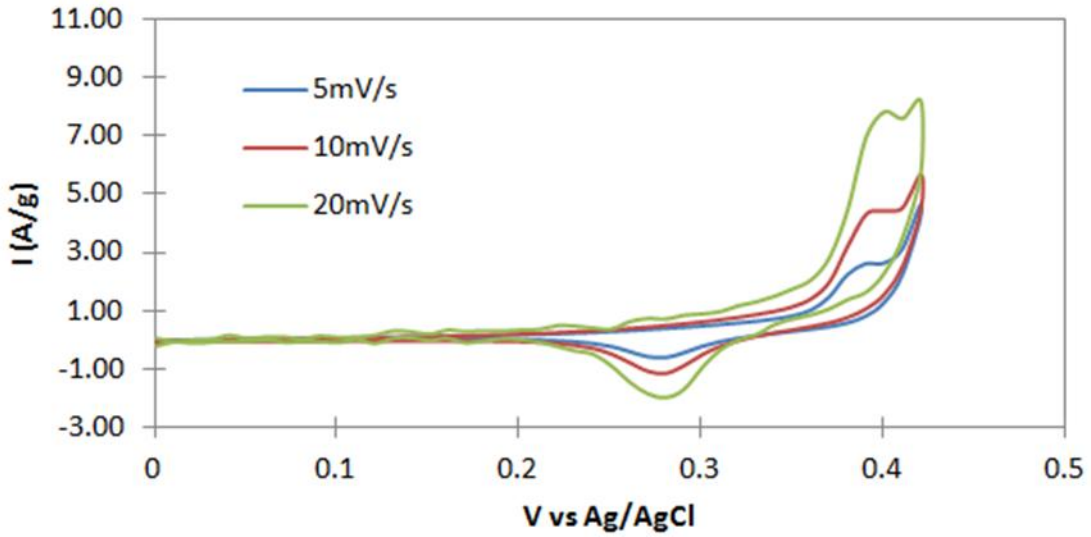

b

Figure 4.3. Scan rate dependent CV of high load NiO nanofibers at (a) 10 mV/s and (b) for the 800℃ treatment.

correspond to the $NiOH_2/NiOH$ redox reaction in the CV according to the following electrochemical reaction:

$$NiO + OH \rightarrow NiOOH + e^- \quad (4.1)$$

It is believed that NiO in contact with alkaline solution tends to change to nickel hydroxide at the surface forming a surface layer onto NiO about several angstroms thick [20, 21]. The proportion of nickel hydroxide formed would be proportional to the area of nickel oxide exposed to the solution. A maximal capacitance ~500 F/g was observed for the 800 ^{o}C-treated NiO (see Fig. 4.4).

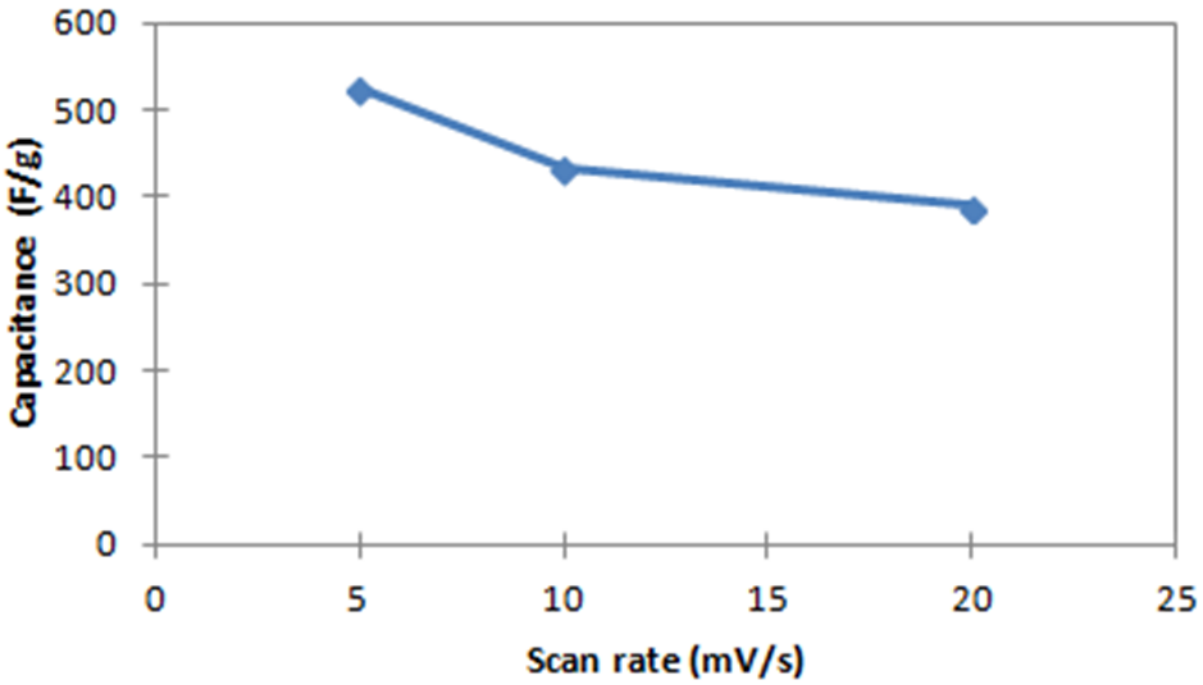

Figure 4.4. Specific capacitance of 800 ^{o}C treated NiO.

Conclusion

Here we demonstrate the pseudocapacitance behavior of high load NiO nanofibers with large crystal domains. Cyclic voltammograms showed clearly resolved peaks with the sample fired at 800 ^{o}C. The presence of macroscopic properties, such as particle size, help enlarge the contact area and electron tunneling length. This ultimately improved the electrode conductivity and enhanced the electrochemical kinetics.

References

[1] Conway, B. E., Birss, V., & Wojtowicz, J. (1997). The role and utilization of pseudocapacitance for energy storage by supercapacitors. *Journal of Power Sources*, *66*(1-2), 1–14.

[2] Ko, R., & Carlen, M. (2000). Principles and applications of electrochemical capacitors. *Electrochimica Acta*, *45*, 2483–2498.

[3] Stoller, M. D., & Ruoff, R. S. (2010). Best practice methods for determining an electrode material's performance for ultracapacitors. *Energy & Environmental Science*, *3*(9), 1294.

[4] Frackowiak, E., & Béguin, F. (2001). Carbon materials for the electrochemical storage of energy in capacitors. *Carbon*, *39*(6), 937–950.

[5] Sun, G., Li, K., & Sun, C. (2010). Electrochemical performance of electrochemical capacitors using Cu(II)-containing ionic liquid as the electrolyte. *Microporous and Mesoporous Materials*, *128*(1-3), 56–61.

[6] Toupin, M., Brousse, T., & Be, D. (2004). Charge Storage Mechanism of MnO 2 Electrode Used in Aqueous Electrochemical Capacitor, (9), 3184–3190.

[7] Sarangapani, S. (1996). Materials for Electrochemical Capacitors. *Journal of The Electrochemical Society*, *143*(11), 3791. doi:10.1149/1.1837291

[8] Hsieh, C.-T., Chou, Y.-W., & Chen, W.-Y. (2007). Synthesis and electrochemical characterization of carbon nanotubes decorated with nickel nanoparticles for use as an electrochemical capacitor. *Journal of Solid State Electrochemistry*, *12*(6), 663–669.

[9] Hu, C.-C., Chang, K.-H., Lin, M.-C., & Wu, Y.-T. (2006). Design and tailoring of the nanotubular arrayed architecture of hydrous RuO2 for next generation supercapacitors. *Nano letters*, *6*(12), 2690–5.

[10] Devadas, A., Baranton, S., Napporn, T. W., & Coutanceau, C. (2011). Tailoring of RuO2 nanoparticles by microwave assisted "Instant method" for energy storage applications. *Journal of Power Sources*, *196*(8), 4044–4053.

[11] P. K. Nayak and N. Munichandraiah, "Mesoporous MnO(2) synthesized by using a tri-block copolymer for electrochemical supercapacitor studies," Microporous and Mesoporous Materials, vol. 143, pp. 206-214, Aug 2011.

[12] P. Ragupathy, et al., "Synthesis and characterization of nano-MnO2 for electrochemical supercapacitor studies," Journal of the Electrochemical Society, vol. 155, pp. A34-A40, 2008.

[13] Gao, H., Ting, Y.-J., Kherani, N. P., & Lian, K. (2013). Ultra-high-rate all-solid pseudocapacitive electrochemical capacitors. *Journal of Power Sources*, *222*, 301–304.

[14] Deng, W., Ji, X., Chen, Q., & Banks, C. E. (2011). Electrochemical capacitors utilising transition metal oxides: an update of recent developments. *RSC Advances*, *1*(7), 1171.

[15] Nathan, T., Aziz, a., Noor, a. F., & Prabaharan, S. R. S. (2007). Nanostructured NiO for electrochemical capacitors: synthesis and electrochemical properties. *Journal of Solid State Electrochemistry*, *12*(7-8), 1003–1009.

[16] Li, Y., Huang, K., Yao, Z., Liu, S., & Qing, X. (2011). Co3O4 thin film prepared by a chemical bath deposition for electrochemical capacitors. *Electrochimica Acta*, *56*(5), 2140–2144.

[17] Hsieh, C.-T., Chou, Y.-W., & Chen, W.-Y. (2007). Synthesis and electrochemical characterization of carbon nanotubes decorated with nickel nanoparticles for use as an electrochemical capacitor. *Journal of Solid State Electrochemistry*, *12*(6), 663–669.

[18] Simon, P., & Gogotsi, Y. (2008). Materials for electrochemical capacitors. *Nature materials*, *7*(11), 845–54.

[19] Saliger, R.; Fischer, U.; Herta, C.; Fricke, J. High Surface Area Carbon Aerogels for Supercapacitors. J. Non-Cryst. Solids 1998, 225, 81-85.

[20] Li, C.; Wang, D.; Liang, T.; Wang, X.; Ji, L. A Study of Activated Carbon Nanotubes as Double-Layer Capacitors Electrode Materials. Materials Letters 2004, 58, 3774-3777.

[21] Ajayan, P. M. Nanotubes from Carbon, Chem. Rev. 1999, 99, 1787-1800.

[22] Ye, J. S.; Liu, X.; Cui, H. F.; Zhang, W. D.; Sheu F. S.; Lim, T. M. Electrochemical Oxidation of Multi-Walled Carbon Nanotubes and its Application to Electrochemical Double Layer Capacitors. Electrochem. Comm. 2005, 7, 249- 255.

[23] Pico, F.; Rojo, J. M.; Sanjuan, M. L.; Anson, A.; Benito, A. M.; Callejas, M.A.; Maser, W. K.; Martinez, M.T. Single-Walled Carbon Nanotubes as Electrodes in Supercapacitors. J. Electrochem. Soc. 2004,151, A831-A837.

[24] Honda, K.; Yoshimura, M.; Kawakita, K.; Fujishima, A.; Sakamoto, Y.; Yasui, K.;NishioN.; Masuda, H. Electrochemical Characterization of Carbon Nanotube/Nanohoneycomb Diamond Composite Electrodes for a Hybrid Anode of Li-Ion Battery and Super Capacitor. J. Electrochem. Soc. 2004,757 A532 -A541

[25] Trasatti, S.; Lodi, S. Electrodes of Conducting Metal Oxides. In Properties of Conductive Transition Metal Oxides With Rutile-Type Structures, Eds.; S. Trasatti, Elsevier, Amsterdam, 1980, pp. 301-358.

[26] Q. Lu, et al., "Supercapacitor Electrodes with High-Energy and Power Densities Prepared from Monolithic NiO/Ni Nanocomposites," Angewandte Chemie-International Edition, vol. 50, pp. 6847-6850, 2011.

[27] Q. Lu, et al., "Differentiation of Bulk and Surface Contribution to Supercapacitance in Amorphous and Crystalline NiO," Chemsuschem, vol. 3, pp. 1367-1370, 2010.

[28] Hansen, N. S., Cho, D., & Joo, Y. L. (2012). Metal nanofibers with highly tunable electrical and magnetic properties via highly loaded water-based electrospinning. *Small (Weinheim an der Bergstrasse, Germany)*, *8*(10), 1510–4.

Chapter 5

Composite Electrochemical Capacitors with Graphene Nanoribbons and Nickel Oxide Nanofibers

Introduction

Electrochemical capacitors used in high energy storage devices utilize either EDLC or pseudocapacitance contributions to generate energy. EDLCs often use high surface area carbon materials to optimize the surface area interactions between the electrode/electrolyte interfaces. Psuedocapacitors often utilize transitional metal oxides with high levels of oxidation to participate in reversible oxidation/reduction reactions that occur near or at the surface of the electrode interface. Here we combine the GNR sample with nickel oxide to form composite carbon/metal oxide electrochemical capacitors to see the effect of the interactions between both species together. Significant research has shown that combination of high surface area carbon materials with metal oxide has increased effects not see in the individual materials alone [1-7].

In this chapter, composite electrodes composed of high load nickel oxide fibers and graphene nanoribbons are generated and studied for the electrochemical capacitance contributions. For this study high load nickel oxide heat treated at 800 ^{o}C in chapter 4 are combined with GNR1 and GNR2 from chapter 3.

Experimental Methods

The nickel oxide electrode was prepared using a standard procedure by mixing NiO/Nafion/GNR in 40:20:40 rations. The electrode was made by dispersing the above mixture in isopropanol and sonicated for 30 minutes to form a slurry. The slurry was then coated on a stainless steel current collector.

An open-beaker three-electrode cell, composed of the active material electrode as a working electrode, Ag/AgCl as the reference electrode, and platinum wire as the counter electrode was set-up. Aqueous 3M KOH was used as electrolyte solution. This experiment was designed to study the redox behavior of the synthesized nickel oxide fibers.

Results and Discussion

The surface morphology of the GNR1 and GNR2 were studied under SEM. The only difference between these two samples is that GNR1 was functionalized while GNR2 was not functionalized. The effects of functionalization can be seen as one that decreases the effect of aggregation as seen in Figure 5.1 where GNR1 tends to form a well dispersed mixture while GNR2 is much more closely packed. The surface area contributions from BET analysis for GNR1 and GNR2 are 38 and 58 m^2/g respectively.

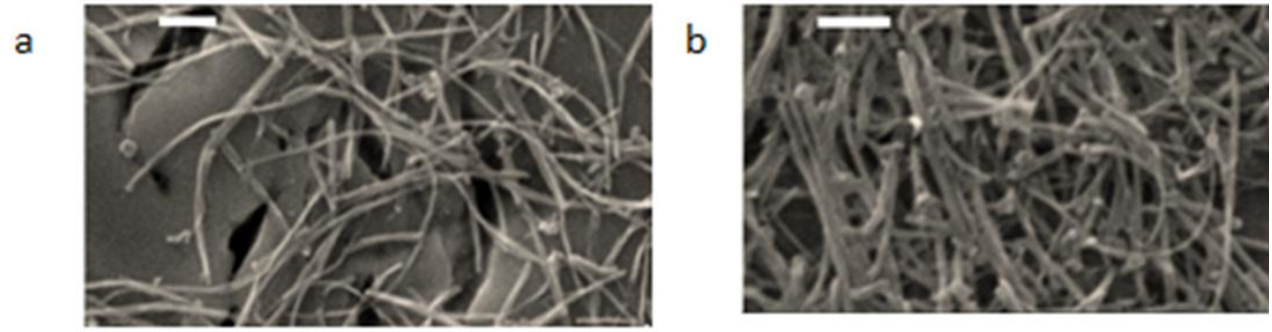

Figure 5.1. SEM Image of (a) GNR1 and (b) GNR2 after sonication.

The nanostructure morphology of the calcined fibers was confirmed by FE SEM analysis. The average fiber diameter at 400 ºC, 600 ºC, and 800 ºC were 300±30 , 270±60, and 250±20 nm respectively. Figure 5.2 clearly demonstrated that as the heat treatment temperature increases the particles grown significantly.

Cyclic voltammetry was used to determine the electrochemical properties of the synthesized NiO nanofibers in 3 M KOH solution. Nickel oxide calcined at 800 °C was chosen for this study since it had the highest performance (see chapter 4). Figure 5.3 shows the rate dependent cyclic voltammetry (CV) of NiO vs Ag/AgCl. The electrode potential was scanned

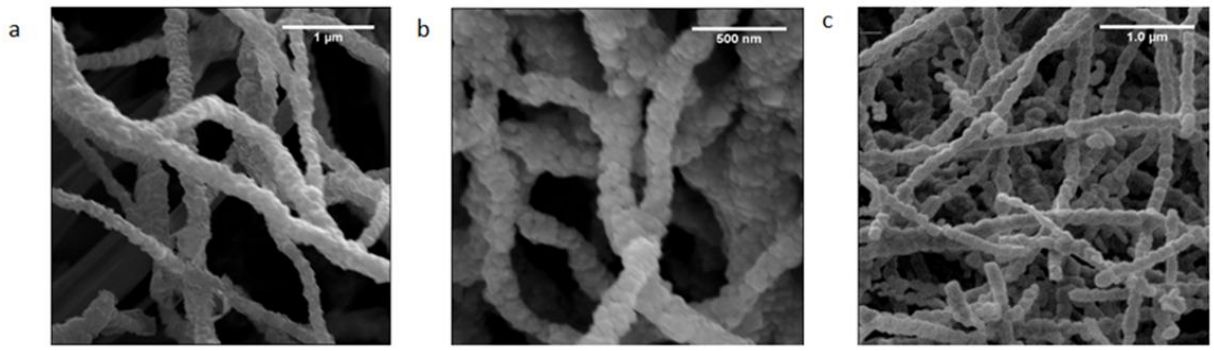

Figure 5.2 FE-SEM Pictures of NiO heated at a 400 °C , b 600 °C, and c 800 °C at 5°C /min for 1 hour in air

between 0.0 and 0.5 V vs Ag/AgCl in both anodic and cathodic directions while the current was measured. The redox features corresponding to anodic and cathodic peaks occur at ~0.38 and 0.26 V respectively at 5 mV/s in the 800 °C NiO case. The incorporation of GNR significantly increases the capacitance of the electrodes. For the pure nickel oxide treated at 800 °C, a high capacitance of ~ 500 F/g is observed. The inclusion of GNR takes that value to above 600 F/g. In particular, there is an interesting shift between GNR1 and GNR2. In GNR1, where the material was functionalized, the larger crystal domain NiO attributed to much higher capacitance (640 F/g). Conversely, in the GNR2 sample where the nanoribbons are much closer together due to some aggregation the interaction between the smaller crystal domain 600C interacts better with the GNR2 for a higher capacitance (660 F/g). Possibly due to the presence of aggregation the 800°C nanowires are not easily accessible to the surface of GNR2 as they are to the surface of GNR1 where aggregation is very limited.

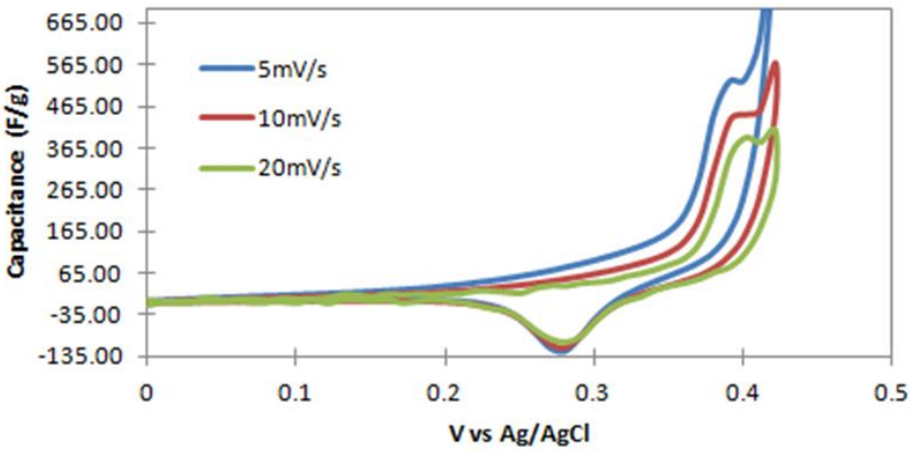
665.00
565.00
465.00
365.00
265.00
165.00
65.00
-35.00
-135.00
Capacitance (F/g)
5mV/s
10mV/s
20mV/s
0
0.1
0.2
0.3
0.4
0.5
V vs Ag/AgCl

a

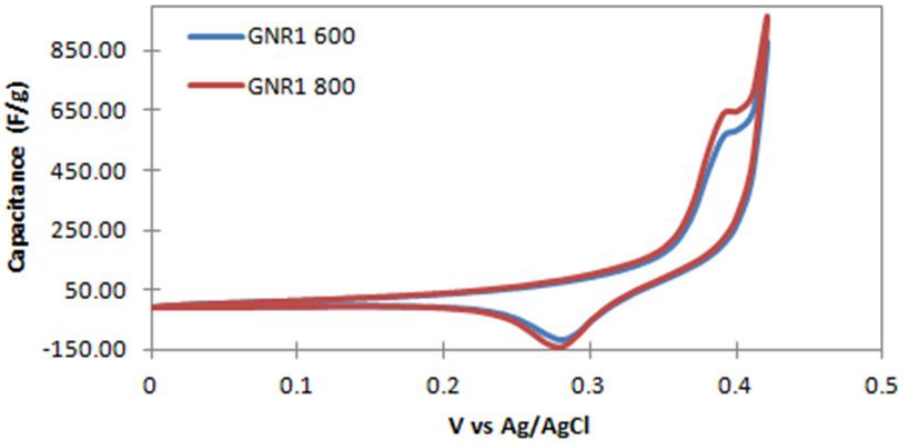
850.00
650.00
450.00
250.00
50.00
-150.00
Capacitance (F/g)
GNR1 600
GNR1 800
0
0.1
0.2
0.3
0.4
0.5
V vs Ag/AgCl

b

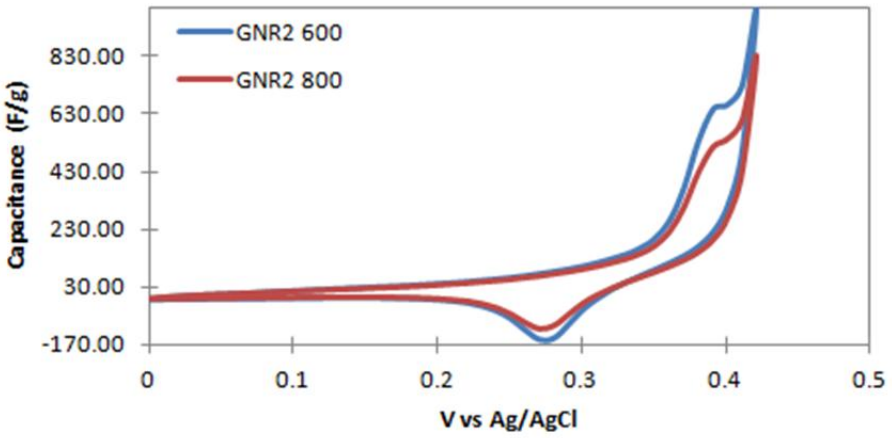

c

Figure 5.3 scan rate dependent CV of a) high load NiO at 800 °C (b)composite NiO/GNR1 and (c) composite NiO/GNR2

Conclusion

Here we demonstrate the pseudocapacitance behavior of high load NiO nanofibers with large and crystal domains interacting with GNR. Cyclic voltammograms showed clearly resolved peaks with the 800 °C treated sample and incorporation of GNR increased the specific capacitance significantly. The presence of macroscopic properties such as particle size facilitate the interaction between the GNR and NiO interface. This ultimately improved the metal oxide/graphene nanoribbon interaction and enhanced the electrochemical performance.

Reference

[1] Kim, S.-U., & Lee, K.-H. (2004). Carbon nanofiber composites for the electrodes of electrochemical capacitors. *Chemical Physics Letters*, *400*(1-3), 253–257. doi:10.1016/j.cplett.2004.10.124

[2] Lee, S. W., Kim, J., Chen, S., Hammond, P. T., & Shao-Horn, Y. (2010). Carbon nanotube/manganese oxide ultrathin film electrodes for electrochemical capacitors. *ACS nano*, *4*(7), 3889–96. doi:10.1021/nn100681d

[3] Hsieh, C.-T., Chou, Y.-W., & Chen, W.-Y. (2007). Synthesis and electrochemical characterization of carbon nanotubes decorated with nickel nanoparticles for use as an electrochemical capacitor. *Journal of Solid State Electrochemistry*, *12*(6), 663–669. doi:10.1007/s10008-007-0399-9

[4] Rakhi, R. B., & Alshareef, H. N. (2011). Enhancement of the energy storage properties of supercapacitors using graphene nanosheets dispersed with metal oxide-loaded carbon nanotubes. *Journal of Power Sources*, *196*(20), 8858–8865. doi:10.1016/j.jpowsour.2011.06.038

[5] Deng, W., Ji, X., Chen, Q., & Banks, C. E. (2011). Electrochemical capacitors utilising transition metal oxides: an update of recent developments. *RSC Advances*, *1*(7), 1171. doi:10.1039/c1ra00664a

[6] Zheng, J. P. (1999). Ruthenium Oxide-Carbon Composite Electrodes for Electrochemical Capacitors. *Electrochemical and Solid-State Letters*, *2*(8), 359. doi:10.1149/1.1390837

[7] Panić, V. V., Stevanović, R. M., Jovanović, V. M., & Dekanski, a. B. (2008). Electrochemical and capacitive properties of thin-layer carbon black electrodes. *Journal of Power Sources*, *181*(1), 186–192. doi:10.1016/j.jpowsour.2008.03.048

Chapter 6

Conclusions and Future Work

Conclusions

The incorporation of high surface area nanostructured materials as a method to optimize the interaction between the solid electrode/electrolyte interface has not directly correlated with improved performance. Although surface area plays a significant role in EC devices, many other factors still interact with the surface that result in drastic deviations in EC performance. Here we conclude that surface area, morphology and crystal size all have an interdependence on capacitance.

Electrochemical double layer capacitors are not simply optimized with the inclusion of high surface area nanostructured devices. Carbon, the most heavily utilized EDLC material, is limited by surface morphology, pore size distribution, as well as surface area. The morphology of the carbon is important. Based on the surface structure after sonication, and the characteristically low CV, the added benefit of high surface area resulted in no significant increase in the performance. By incorporating graphene nanoribbons with much lower surface area a high capacitance value was attained. Furthermore, as the contribution to pores within the 2-3 nm range increased there was an added increase in the performance of the capacitance. As such we must conclude one of two things. Either the contribution due to the large pores significantly limit the performance or the effect of aggregation steadily decreases the performance. Since the other GNR2 and GNR3 did show increased performance with increased surface area one can conclude that a combination of large pores and aggregations does not significantly contribute to beneficial capacitance performance.

Furthermore, a novel approach towards the effects of crystal size in electrochemical capacitors is done through the inclusion of highly loaded nickel oxide nanowires with controllable particle size. Significant work has demonstrated that crystal size plays an important role in electrochemical capacitance performance but most work has been limited to studying the crystal size through nanoparticles or thin film methods. Here we perform a similar study but within the nanowire matrix. This lead to an interesting finding that is different from what has been concluded in nanoparticle systems. In nanoparticle systems, huge grain boundaries tend to limit the transport properties of electrons and conductive mediums. However as you shift to very small particles you create a network that can better facilitate easy transport. However in our nanowire systems, the large crystals formed maintain a coherent matrix which required relatively no hopping and a smooth transport path. Earlier work by Dr. Hansen proved that the incorporation of highly loaded Ni fiber systems lead to increased conductivity. As such, by using the same framework, the incorporation of highly loaded NiO systems benefits from a conductive matrix to facilitate electron transfer. This led to a high capacitance of 500 F/g.

Finally, we investigated the synergy between NiO and graphene nanoribbons to see the combined effect. Here we demonstrated that NiO particles had lower performance when the nanoribbons tended to be in a more aggregated state. While in GNR samples that had relatively low aggregation interacted more favorable with the large NiO crystals. The combined NiO/GNR system increased the capacitance by ~150 F/g for a relatively high capacitance of 650 F/g.

Suggested Future Work

Single Fiber Characterization

Highly loaded NiO nanowires with large crystal matrix performed well within the confines of our three electrode system. However, the driving force or characteristic properties of such materials are not fully understood. Therefore, one could envision that characterizing the electrical conductivity of various high and low load samples to understand the interplay between large and small crystal domain as a possible route to further continue. This can be done in a variety of different ways. The utilization of high resolution AFM to measure the conductivity of single fibers is an interesting approach to gauge the characteristic of single fiber properties. In this approach the AFM can be used to study the electrical and mechanical properties of the fibers Furthermore, one could design a two-electrode system on micro-chip to test the conductivity of single fiber.

Two Electrode Device Fabrication

From an applications point of view, the most feasible path forward would be to design these systems into actual button cells that simulate a realistic version of a battery. The capacitance values generated here appear to be fairly high but once they are incorporated into 2 electrode setup the values tend to decrease drastically from what they are in the three electrode case.

The shift to a two electrode setup also allows for the fabrication of hybrid systems. Currently we have demonstrated the utilization of carbon and metal oxide fibers for EC performances but our work can further expand to asymmetric systems. In this scheme one can envision a device that uses one electrode as NiO and the second electrode as GNR in a combined

cell. This will allow us to study the interplay between each of the electrode for its advantages as a cathode or anode materials.

Finally, in a two electrode setup we can begin to study hybrid energy storage devices. Currently in attempt to increase the capacitance we are utilizing pseudocapacitance materials like NiO and other transitional metals. An alternative approach would be to combine high surface area carbon as the positive electrode with a lithium-air anode material. The ultimate goal would be to combine lithium air materials with characteristically high energy density with EC materials that have characteristically high power density. This should allow for materials that can optimize both of those parameters combined in one device.